Supplementary Material

Emergence of Alterferrimagnetism: A New Magnetic Phase

Chanchal K. Barman[⋆],[1,*] Bishal Das[⋆],[2,†] Alessio Filippetti,[1,3] Aftab Alam,[2,‡] and Fabio Bernardini[1]

[1] *Dipartimento di Fisica, Università di Cagliari, Cittadella Universitaria, Monserrato (CA) 09042, Italy*
[2] *Department of Physics, Indian Institute of Technology Bombay, Mumbai 400076, India*
[3] *CNR-IOM, Istituto Officina dei Materiali, Consiglio Nazionale delle Ricerche, Monserrato, CA 09042-I, Italy*

CONTENTS

⋆ These authors contributed equally to this work.
* arckb2@gmail.com
† dasbishal98@gmail.com
‡ aftab@iitb.ac.in

Here, we briefly recapitulate concepts of group theory and crystallography and present further information on all possible spin arrangements in $CuFePO_5$. We follow the *International Tables of Crystallography, Volume A* (ITA) settings [1, 2] while denoting the crystallographic space groups. The same convention is extended for denoting the spin space groups to avoid possible ambiguities.

SI. REVIEW OF SPIN SPACE GROUPS AND ALTERMAGNETISM

Here we briefly review several key concepts and notations of spin space groups, which have been used extensively in this work, and elucidate how altermagnetism has been defined in the literature on the basis of spin space group [3–10].

A. Fundamentals of Spin Space Groups

The underlying crystalline Bravais lattice of a material is described by *polar* vectors residing in a three-dimensional (3D) Euclidean vector space, the position space. Similarly, the reciprocal Bravais lattice is then described by *polar* vectors residing in an *isomorphic* 3D Euclidean vector space, the momentum space. The position and momentum spaces are collectively termed as the *real-space*. In a crystalline magnetic material, the interacting magnetic moments of basis atoms, primarily arising due to spins of unpaired electrons, give rise to a magnetic order with a definite "spin arrangement" in the crystalline lattice. Treating the moments (spins) as *axial* vectors in yet another 3D Euclidean vector space, termed the *spin-space*, the spin arrangement dictates how spins in a magnetic material are spatially arranged, essentially providing a mapping between two vector spaces— *spin-space* and *real-space* (encompassing both position and momentum spaces). Since the magnetic atoms themselves are spatially arranged in a crystalline lattice, the spin arrangement becomes coupled to the crystal. Magnetic space groups (MSGs) are used to describe the symmetries of magnetic materials which leave the spin arrangement in a crystal invariant. Within the MSG framework, the symmetry transformations act simultaneously on the basis atoms in the *real-space* as well as on the spins in the *spin-space* and is evidently a consequence of SOC, meaning both of these vector spaces no longer remain independent of each other. But in materials with weak or negligible SOC, *real-space* and *spin-space* may be considered as decoupled, giving rise to certain symmetry transformations which act separately on these two vector spaces and also keeps the spin arrangement in a crystal invariant. This leads to a generalization of the MSGs where the symmetry transformations acting on *real-space* and *spin-space* are not necessarily the same resulting in the spin space groups (SSGs). Since SSGs also keep the spin arrangement in a crystal invariant, MSGs form subgroups of SSGs. Henceforth, these groups shall be denoted by boldfaced letters.

Let us now define the SSGs in a mathematically rigorous manner. Formally, a spin space group $\boldsymbol{\mathcal{G}}$ is obtained by taking the *external* direct product of a group of transformations $\mathbb{S}$ residing in the *spin-space* and another group $\mathbb{X}$ residing in the *real-space*, i.e., $\boldsymbol{\mathcal{G}} = \mathbb{S} \otimes \mathbb{X}$. Let us now define the subgroups $\boldsymbol{\mathcal{S}} \subseteq \mathbb{S}$ and $\mathbf{X} \subseteq \mathbb{X}$ such that $\mathbb{S}$ and $\mathbb{X}$ can be respectively partitioned into disjoint sets called cosets. If $\boldsymbol{\mathcal{S}}$ and $\mathbf{X}$ are further considered to be *normal* in $\mathbb{S}$ and $\mathbb{X}$ (denoted by $\boldsymbol{\mathcal{S}} \triangleleft \mathbb{S}$ and $\mathbf{X} \triangleleft \mathbb{X}$) respectively, then the set of corresponding disjoint cosets also form a group yielding the quotient groups $\mathbb{S}/\boldsymbol{\mathcal{S}}$ and $\mathbb{X}/\mathbf{X}$. Choosing $\boldsymbol{\mathcal{S}} \triangleleft \mathbb{S}$ and $\mathbf{X} \triangleleft \mathbb{X}$ such that the quotient groups are *isomorphic* ($\mathbb{S}/\boldsymbol{\mathcal{S}} \cong \mathbb{X}/\mathbf{X}$), the *isomorphic* coset decomposition of $\mathbb{S}$ and $\mathbb{X}$ is given by:

$$\begin{aligned} \mathbb{S} &= \ \mathsf{s}_1\boldsymbol{\mathcal{S}} \cup \mathsf{s}_2\boldsymbol{\mathcal{S}} \cup ... \cup \mathsf{s}_n\boldsymbol{\mathcal{S}} \quad (\mathsf{s}_i \in \mathbb{S}\ \forall i = 1, ..., n) \\ \mathbb{X} &= \ \mathsf{x}_1\mathbf{X} \cup \mathsf{x}_2\mathbf{X} \cup ... \cup \mathsf{x}_n\mathbf{X} \quad (\mathsf{x}_i \in \mathbb{X}\ \forall i = 1, ..., n) \end{aligned}$$

Here, n is the total number of distinct cosets corresponding to a subgroup and is referred to as the *index* of the subgroup in the parent group. Pairing the elements of the cosets $\mathsf{s}_i\boldsymbol{\mathcal{S}}$ and $\mathsf{x}_i\mathbf{X}$, the group elements of $\boldsymbol{\mathcal{G}}$ are obtained using the *isomorphism* theorem for groups [3] as an ordered pair $[\,\mathsf{s}_i\,||\,\mathsf{x}_i\,]$, where $\mathsf{s}_i \in \mathbb{S}$ and $\mathsf{x}_i \in \mathbb{X}$ (s_1 and x_1 are identities of $\mathbb{S}$ and $\mathbb{X}$ respectively). Then the full SSG can be written as:

$$\boldsymbol{\mathcal{G}} = \mathbb{S}\otimes\mathbb{X} = [\boldsymbol{\mathcal{S}}||\mathbf{X}] \cup [\mathsf{s}_2\boldsymbol{\mathcal{S}}||\mathsf{x}_2\mathbf{X}] \cup ... \cup [\mathsf{s}_n\boldsymbol{\mathcal{S}}||\mathsf{x}_n\mathbf{X}] \tag{S.1}$$

Thus to construct a spin space group $\boldsymbol{\mathcal{G}}$, it is imperative to find or choose subgroups $\boldsymbol{\mathcal{S}}$ and $\mathbf{X}$ such that they are *normal* in $\mathbb{S}$ and $\mathbb{X}$ respectively. It is only under this condition that the set of cosets will form quotient groups and the *isomorphic* coset decomposition can be performed.

We now look at the structure of $\boldsymbol{\mathcal{G}}$ in more detail [3–7]. In a SSG, there exists transformations of the *spin-space* alone of the form $[\,\mathfrak{R}\,||\,\mathbb{I}\,]$. These transformations yield a *normal* subgroup $\boldsymbol{\mathfrak{G}}_{\mathbf{S}} \triangleleft \boldsymbol{\mathcal{G}}$ called the spin-only group. All other transformations which act on both *real-space* and *spin-space* form yet another *normal* subgroup $\boldsymbol{\mathcal{G}}_{\mathbf{S}} \triangleleft \boldsymbol{\mathcal{G}}$ called the non-trivial spin group. They are of the general form $[\,\mathfrak{Q}\,||\,R\,]$ and do not contain any elements of the form

$[\mathfrak{R}\,||\,\mathbb{I}] \in \mathfrak{G}_\mathbf{S}$ except the group identity $[\mathfrak{I}\,||\,\mathbb{I}]$. Here, $\mathfrak{I}$ is the *spin-space* identity and $\mathbb{I}$ is the *real-space* identity. Also, the transformations $\mathfrak{R}$ and R act exclusively on the *spin-space* and *real-space* respectively. Since both $\mathfrak{G}_\mathbf{S}$ and $\mathbb{G}_\mathbf{S}$ are *normal* in $\mathcal{G}$, an alternate way of characterizing $\mathcal{G}$ is by the *internal* direct product $\mathcal{G} = \mathfrak{G}_\mathbf{S} \times \mathbb{G}_\mathbf{S}$ with group elements denoted by $[\mathfrak{R}\,||\,R]$. The spin-only group $\mathfrak{G}_\mathbf{S}$ depends only on the type of spin arrangement in a magnetic crystal and is common to all SSGs since it is independent of any *real-space* transformations. By contrast, the non-trivial spin group $\mathbb{G}_\mathbf{S}$ depends on the crystal itself via the crystallographic space group $\mathbf{G}$ since $R \in \mathbf{G}$ and distinguishes the different SSGs for a particular spin arrangement. Hence, finding the non-trivial spin groups is sufficient to enumerate and construct all possible SSGs. The primary definition of a SSG is that it must leave the spin arrangement in a crystal invariant and since both $\mathfrak{G}_\mathbf{S}$ and $\mathbb{G}_\mathbf{S}$ are SSGs by themselves, this leads to the following interesting consequences. The *spin-space* transformations $\mathfrak{R}$ of $[\mathfrak{R}\,||\,\mathbb{I}] \in \mathfrak{G}_\mathbf{S}$ can keep a spin arrangement invariant even without considering any *real-space* transformations. These underlying *spin-space* transformations form a *normal* subgroup $\boldsymbol{\mathcal{S}} \triangleleft \mathbb{S}$, i.e., $\mathfrak{R} \in \boldsymbol{\mathcal{S}}$. By contrast, the *spin-space* transformations $\mathfrak{Q}$ of $[\mathfrak{Q}\,||\,R] \in \mathbb{G}_\mathbf{S}$ are able to keep a spin arrangement invariant only in conjunction with the *real-space* transformations R since $[\mathfrak{R}\,||\,\mathbb{I}] \notin \mathbb{G}_\mathbf{S}\ \forall\, \mathfrak{R} \in \boldsymbol{\mathcal{S}}$, except $[\mathfrak{I}\,||\,\mathbb{I}]$. These underlying *spin-space* transformations form yet another *normal* subgroup $\widetilde{\boldsymbol{\mathcal{S}}} \triangleleft \mathbb{S}$ such that $\boldsymbol{\mathcal{S}} \cap \widetilde{\boldsymbol{\mathcal{S}}} = \{\mathfrak{I}\}$ and $\mathfrak{Q} \in \widetilde{\boldsymbol{\mathcal{S}}}$. Thus, $\mathbb{G}_\mathbf{S}$ can be written in a form analogous to Eq. (S.1):

$$\mathbb{G}_\mathbf{S} = \widetilde{\boldsymbol{\mathcal{S}}} \otimes \mathbf{G} \tag{S.2}$$

The elements of $\mathbb{G}_\mathbf{S}$ are then obtained from an *isomorphic* coset decomposition of the group of *spin-space* transformations $\widetilde{\boldsymbol{\mathcal{S}}}$ and the crystallographic space group $\mathbf{G}$ such that the parent group of *spin-space* transformations is then given by $\mathbb{S} = \boldsymbol{\mathcal{S}} \times \widetilde{\boldsymbol{\mathcal{S}}}$ [3].

B. Classification of Altermagnetism using Spin Space Groups

For collinear spin arrangements, the group of underlying *spin-space* transformations of $\mathfrak{G}_\mathbf{S}$ is given by $\boldsymbol{\mathcal{S}} = \boldsymbol{\mathcal{C}}_\infty \cup \overline{\mathfrak{C}}_2 \boldsymbol{\mathcal{C}}_\infty$ [3, 6, 7, 11]. Here, $\boldsymbol{\mathcal{C}}_\infty$ is the special orthogonal group of rotations about the common axis of all collinear magnetic moments in the *spin-space* which keeps any collinear spin arrangement invariant. The *spin-space* transformation $\overline{\mathfrak{C}}_2 = \mathcal{T}\mathfrak{C}_2$ is a 2-fold rotation in the *spin-space* about an axis perpendicular to the common axis followed by time-reversal. Both $\mathfrak{C}_2$ and $\mathcal{T}$ act as spin inversion flipping the collinear spins, and their combined action keeps the spin arrangement invariant. Time-reversal additionally acts on the *real-space* since $\mathcal{T}$ also reverses momenta although $[\overline{\mathfrak{C}}_2\,||\,\mathcal{T}] \in \mathfrak{G}_\mathbf{S}$ where $\overline{\mathfrak{C}}_2 \in \boldsymbol{\mathcal{S}}$. Then for collinear spin arrangement, there arises two possibilities of choosing $\widetilde{\boldsymbol{\mathcal{S}}}$, the group of underlying *spin-space* transformations of $\mathbb{G}_\mathbf{S}$.

The first possibility is that all *spin-space* transformations keep the collinear spin arrangement invariant irrespective of the presence of any *real-space* transformations, implying $\boldsymbol{\mathcal{S}}$ constitutes the group of all *spin-space* transformations and $\widetilde{\boldsymbol{\mathcal{S}}} = \{\mathfrak{I}\}$ is the trivial group. Here, there is no operation which can explicitly flip spins leading to only same-spin sublattice transformations that keep the collinear spin arrangement invariant. Thus $\mathbb{G}_\mathbf{S}$ can be constructed only from *isomorphic* one-coset decompositions of *spin-space* transformation $\widetilde{\boldsymbol{\mathcal{S}}} = \{\mathfrak{I}\}$ and crystallographic space group $\mathbf{G}$ defining Type-I SSGs which explicitly break $\mathcal{T}$. These transformations produce a momentum-independent isotropic spin splitting throughout the Brillouin zone, characteristic of the ferromagnetic phase.

The other possibility is to consider a *spin-space* operation that can flip spins, yet keep the spin arrangement invariant. The natural choice is either $\mathfrak{C}_2$ or $\mathcal{T}$ and we choose $\mathfrak{C}_2$ since it exclusively acts on the *spin-space* unlike $\mathcal{T}$, although both choices ultimately lead to the same $\mathcal{G}$. But it is important to note that flipping spins in a collinear spin arrangement can never keep it invariant unless the *spin-space* transformation acts in conjunction with some *real-space* transformation such that the original spin arrangement is recovered. Thus, $\mathbb{G}_\mathbf{S}$ can be constructed from $\widetilde{\boldsymbol{\mathcal{S}}} = \{\mathfrak{I}, \mathfrak{C}_2\}$ and $\mathbf{G}$ (see eq. (S.2)). Interestingly, there are two different *isomorphic* coset decompositions possible because now $\widetilde{\boldsymbol{\mathcal{S}}}$ is no longer the trivial group. For an *isomorphic* one-coset decomposition, the resulting $\mathbb{G}_\mathbf{S}$ and consequently the full SSG $\mathcal{G}$ preserves $\mathcal{T}$ defining Type-II SSGs. These transformations produce fully spin-degenerate dispersion throughout the Brillouin zone, characteristic of the antiferromagnetic phase.

But for an *isomorphic* two-coset decomposition, there arises two further possibilities. Let us assume that $\mathbf{G}$ contains a subgroup $\mathbf{H}$ of *index* 2, also called a *halving* subgroup, with the coset decomposition $\mathbf{G} = \mathbf{H} \cup R\mathbf{H} = \mathbf{H} \cup (\mathbf{G} - \mathbf{H})$, where R is a coset-representative such that $R \notin \mathbf{H}$ but $R \in \mathbf{G}$. In general, $\mathbf{G}$ can either be centrosymmetric ($\mathcal{P} \in \mathbf{G}$) or non-centrosymmetric ($\mathcal{P} \notin \mathbf{G}$) and depending on R, the two-coset decomposition leads to two distinct $\mathbb{G}_\mathbf{S}$. For either $R = \mathcal{P}$ or $R = t$, the resulting $\mathbb{G}_\mathbf{S}$ reduces to that of the Type-II SSGs [6, 7]. But if $R \neq \mathcal{P}$ and $R \neq t$ (R could be non-symmorphic, i.e, may contain t combined with rotations or reflections), $\mathcal{T}$ is explicitly broken in the resulting $\mathcal{G}$, yielding Type-III SSGs. These transformations produce momentum-dependent anisotropic spin splitting with alternating spin-polarized dispersions in the Brillouin zone, characteristic of the altermagnetic phase [6, 7]. Thus, the *halving* subgroup of a parent crystallographic space group plays a central role in determining the AM phase.

The first and foremost condition for obtaining an AM phase (Type-III SSG) is the existence of a *halving* subgroup **H**, which by construction is a *normal* subgroup, such that an *isomorphic* two-coset decomposition is possible and which generates all the same-spin sublattice transformations. This also implies that the set of all transformations that map the same spins must follow group axioms. The coset $\mathbf{G}-\mathbf{H}$ will then generate all the opposite-spin sublattice transformations. In general, there could be more than one *halving* subgroup and if **G** does not have any *halving* subgroup, then AM phase cannot be achieved in such crystallographic space groups. Any space group with the underlying point group as **1** ($\boldsymbol{C_1}$), **3** ($\boldsymbol{C_3}$) or **23** ($\boldsymbol{T}$) falls under this category. As noted earlier, AM phase will be achieved in a centrosymmetric space group *iff* $\mathcal{P}, t \notin (\mathbf{G}-\mathbf{H})$ or equivalently $\mathcal{P}, t \in \mathbf{H}$. The centrosymmetric space groups with the underlying point group as $\overline{\mathbf{1}}$ ($\boldsymbol{C_i}$), $\overline{\mathbf{3}}$ ($\boldsymbol{C_{3i}}$ or $\boldsymbol{S_6}$) or $\boldsymbol{m\overline{3}}$ ($\boldsymbol{T_h}$) do not satisfy these conditions and hence cannot yield AM phase. For non-centrosymmetric space groups, the condition $\mathcal{P} \notin (\mathbf{G}-\mathbf{H})$ is satisfied trivially and hence AM phase may be achieved *iff* $t \notin (\mathbf{G}-\mathbf{H})$. This final condition is trivially satisfied for space groups with *primitive* Bravais lattices, which are denoted starting with P in the Hermann-Mauguin notation [2]. But for *centered* Bravais lattices, i.e., space groups beginning with F (face-centered), I (body-centered), R (rhombohedral) or A, B, C (base-centered) in the Hermann-Mauguin notation [2], $t \notin (\mathbf{G}-\mathbf{H})$ may not be satisfied due to the existence of non-trivial *centering* lattice translations. This is further discussed in Sec. SII B. In the following discussions, we shall be primarily using the Schönflies notation [2] for denoting the crystallographic space groups and point groups since it is compact and occasionally use the Hermann-Mauguin notation [2] when the space group needs to be distinguished explicitly.

C. Momentum-dependent Spin-splitting in Altermagnets

The defining signature of the AM phase is the presence of momentum-dependent anisotropic spin-splitting of electronic bands. Since our aim is to understand symmetries responsible for such spin-split dispersion in the momentum ($\vec{k}$) space, it suffices to consider only the point group symmetry operations without any loss of generality, i.e., screw operations reduce to simple rotations and glide reflections reduce to simple reflections. This is because any fractional translation in *real-space* generates a multiplicative phase factor in the electronic wavefunction which does not change the corresponding energy eigenvalue. The *real-space* transformations are provided by the *isomorphic* point group of the crystallographic space group **G** whereas the *spin-space* transformations are provided by underlying $\widetilde{\boldsymbol{\mathcal{S}}}$ of $\mathbb{G}_{\mathbf{S}}$ such that $\widetilde{\boldsymbol{\mathcal{S}}} = \{\mathfrak{I}, \mathfrak{C}_2\}$ for the AM phase (see Sec. SI) [6, 7]. Since AMs show momentum-dependent spin-splitting, it is imperative to find the subset of symmetries that enforces spin degeneracies. This can only arise from transformations that exchange atoms belonging to opposite-spin sublattice. Considering a generic crystal momentum $\vec{k} = (k_x, k_y, k_z)$, the action of $R \in \mathbf{G}-\mathbf{H}$ leads to $\vec{k}' = R\,\vec{k}$. Labeling the energy eigenvalues by $\varepsilon_j(\sigma, \vec{k})$, with j the band index and σ the spin, the action of opposite-spin sublattice transformations takes the form:

$$[\mathfrak{C}_2 \,||\, R]\;\; \varepsilon_j(\sigma, \vec{k}) = \varepsilon_j(-\sigma, \vec{k}') \Rightarrow \varepsilon_j(\sigma, \vec{k}) = \varepsilon_j(-\sigma, \vec{k}') \tag{S.3}$$

If R leaves $\vec{k}$ invariant up to a reciprocal lattice vector $\vec{g}$, i.e., $\vec{k}' = \vec{k} + \vec{g}$ implying R belongs to the little group ($\mathcal{L}_{\vec{k}}$) of $\vec{k}$, then Eq. (S.3) enforces spin-degeneracy of energy bands. Else the energy bands become spin-split along momentum directions related by R leading to alternating spin polarization, hallmark of the AM phase.

SII. COMPATIBILITY OF WYCKOFF POSITIONS IN ALTERMAGNETS

A. Wyckoff Positions and *Site-symmetry* Groups

In the main manuscript, we discuss how the *site-symmetry* groups of Wyckoff positions play a central role in determining *compatibility* with Altermagentism. Here, we recapitulate a few important definitions from crystallography [2] related to the *site-symmetry* groups. Each and every point in a crystalline lattice is subject to the symmetry operations of its crystallographic space group **G**. These operations either map the point onto itself or onto another symmetry-equivalent point within the lattice. The *set* of distinct lattice points to which a particular lattice point is mapped to by all the symmetry operations in **G** is known as the *crystallographic orbit* of that lattice point. The *site-symmetry* group **W** of a lattice point is a group that leaves that particular point invariant in the lattice, i.e., maps the point onto itself (up to a trivial lattice translation) and is necessarily *isomorphic* to a subgroup of the underlying point group corresponding to **G**. This means no fractional lattice translations can exist in **W**. It is important to note here that two distinct lattice points may have the same **W** but different *crystallographic orbits*. This leads to the notion of Wyckoff positions which are classes of *crystallographic orbits*. Within a given Wyckoff position, the

site-symmetry group $\mathbf{W}$ of every lattice point is conjugate to each other, and the number of such distinct lattice points in the *crystallographic orbit* defines the multiplicity of that Wyckoff position. Different Wyckoff positions may share the same $\mathbf{W}$ and hence have the same multiplicity but they will always correspond to different *crystallographic orbits*. While lattice points within a single Wyckoff position are symmetry-equivalent, points belonging to different Wyckoff positions cannot be related by any space group operations. In some cases, translations which belong to the *affine normalizer* of the crystallographic space group may connect points across different Wyckoff positions and a detailed discussion on this lies beyond the scope of the present work. For space groups with *primitive* Bravais lattices, the Wyckoff positions with multiplicity 2 have *site-symmetry* groups *isomorphic* to a *halving* subgroup of the parent crystallographic space group, denoted by $\mathbf{W} \cong \mathbf{H}$. But for space groups with *centered* Bravais lattices, the multiplicity of such Wyckoff positions will be twice of the number of *centering* translations because the *centering* translations can never be in $\mathbf{W}$.

B. Sufficient Conditions for Altermagnetism

The Fundamental Lemma of Altermagnetism (FLAM) has been stated and proven in Sec. II of the main manuscript. Here, we discuss the sufficient conditions required for the existence of AM phase in a magnetic crystalline material. Although *even* multiplicity and $\mathbf{W} \subseteq \mathbf{H} \triangleleft \mathbf{G}$ as stated in FLAM form the necessary conditions of AM phase, they are not sufficient to completely assert the existence of the AM phase even if magnetic species occupy the *compatible* Wyckoff positions with a compensated spin arrangement. While it is an implicit requirement that the set of same-spin sublattice transformations must follow group axioms for a given spin arrangement, one must additionally take into account the underlying Bravais lattice of $\mathbf{G}$, and whether $\mathbf{G}$ is centrosymmetric or not, resulting in the following distinct cases:

1. Space groups with *primitive* Bravais lattices ($t \notin \mathbf{G}$):
   These space groups, beginning with P in the Hermann-Mauguin notation [2], consist of only trivial (*primtive*) lattice translations.

   i) Centrosymmetric space groups ($\mathcal{P} \in \mathbf{G}$) will have the following two subcases—
   - If $\mathcal{P} \in \mathbf{W}$, then distinct lattice points in the same *crystallographic orbit* can never be mapped by $\mathcal{P}$. The condition $\mathcal{P}, t \notin (\mathbf{G} - \mathbf{H})$ is satisfied trivially meaning $\mathbf{H}$ can always be constructed from $\mathbf{W}$ for any compensated spin arrangement at the corresponding Wyckoff position provided the set of same-spin sublattice transformations form a group. Wyckoff positions like these will always be *compatible* with the AM phase.
   - If $\mathcal{P} \notin \mathbf{W}$, then distinct lattice points in the same *crystallographic orbit* will be mapped by $\mathcal{P}$. Although the condition $t \notin (\mathbf{G} - \mathbf{H})$ is satisfied trivially, the AM phase will exist *iff* a $\mathbf{H}$ can be constructed from $\mathbf{W}$ and the set of same-spin sublattice transformations absent in $\mathbf{W}$ such that $\mathcal{P} \notin (\mathbf{G} - \mathbf{H})$. Not all compensated spin arrangement at the corresponding Wyckoff position will yield the AM phase. Wyckoff positions like these are not always *compatible* with the AM phase.

   ii) For non-centrosymmetric space groups ($\mathcal{P} \notin \mathbf{G}$), the condition $\mathcal{P}, t \notin (\mathbf{G} - \mathbf{H})$ is satisfied trivially meaning $\mathbf{H}$ can always be constructed from $\mathbf{W}$ for any compensated spin arrangement at the corresponding Wyckoff position provided the set of same-spin sublattice transformations form a group. Wyckoff positions like these will always be *compatible* with the AM phase.

2. Space groups with *centered* Bravais lattices ($t \in \mathbf{G}$):
   These space groups, beginning with F (face-centered), I (body-centered), R (rhombohedral) or A, B, C (base-centered) in the Hermann-Mauguin notation [2], contain *centering* translations t which are non-trivial lattice translations. These translations can never map a distinct lattice point to itself and hence $t \notin \mathbf{W}$ for any $\mathbf{W} \subseteq \mathbf{G}$.

   i) Centrosymmetric space groups ($\mathcal{P} \in \mathbf{G}$) will have the following two subcases—
   - If $\mathcal{P} \in \mathbf{W}$, then distinct lattice points in the same *crystallographic orbit* can never be mapped by $\mathcal{P}$. Although the condition $\mathcal{P} \notin (\mathbf{G} - \mathbf{H})$ is satisfied trivially, the *centering* translations t will map distinct lattice points in the same *crystallographic orbit*. The AM phase will exist *iff* a $\mathbf{H}$ can be constructed from $\mathbf{W}$ and the set of same-spin sublattice transformations absent in $\mathbf{W}$ such that $t \notin (\mathbf{G} - \mathbf{H})$. Not all compensated spin arrangement at the corresponding Wyckoff position will yield the AM phase. Wyckoff positions like these are not always *compatible* with the AM phase.
   - If $\mathcal{P} \notin \mathbf{W}$, then distinct lattice points in the same *crystallographic orbit* will be mapped by $\mathcal{P}$, as well as the *centering* translations t. The AM phase will exist *iff* a $\mathbf{H}$ can be constructed from $\mathbf{W}$ and the set of

same-spin sublattice transformations absent in $\mathbf{W}$ such that $\mathcal{P}, t \notin (\mathbf{G}-\mathbf{H})$. Not all compensated spin arrangement at the corresponding Wyckoff position will yield the AM phase. Wyckoff positions like these are not always *compatible* with the AM phase.

ii) For non-centrosymmetric space groups ($\mathcal{P} \notin \mathbf{G}$), the condition $\mathcal{P} \notin (\mathbf{G}-\mathbf{H})$ is satisfied trivially. But the *centering* translations t will map distinct lattice points in the same *crystallographic orbit*. The AM phase will exist *iff* a $\mathbf{H}$ can be constructed from $\mathbf{W}$ and the set of same-spin sublattice transformations absent in $\mathbf{W}$ such that $t \notin (\mathbf{G}-\mathbf{H})$. Not all compensated spin arrangement at the corresponding Wyckoff position will yield the AM phase. Wyckoff positions like these are not always *compatible* with the AM phase.

The above cases form the sufficient conditions for existence of the AM phase in a magnetic crystalline material. Wyckoff positions that are *compatible* with the AM phase for any compensated spin arrangement shall be referred to as being *fully compatible* with the AM phase. Those Wyckoff positions that are *compatible* with the AM phase for specific compensated spin arrangements shall be referred to as being *partially compatible* with the AM phase. A summary of these necessary and sufficient conditions have been shown in Fig. 2 of main manuscript.

SIII. HYPOTHETICAL ALTERMAGNETS

The metal-oxide iron phosphate family of compounds $MFePO_5$ (M=Cu,Fe,Ni,Co) are comprised of two distinct magnetic species M and Fe, each showing altermagnetism within the M-sublattice and the Fe-sublattice. In Sec. III of the main manuscript, $CuFePO_5$ was chosen as a representative of this family and to better understand alterferrimagnetism in $CuFePO_5$ due to the underlying two interpenetrating altermagnets, we had initially considered two hypothetical compounds by replacing either Cu or Fe. Here, we discuss in detail the altermagnetism due to each magnetic sublattice.

A. $CuGaPO_5$

The hypothetical compound $CuGaPO_5$ is obtained by replacing Fe with Ga in $CuFePO_5$ so as to maintain charge neutrality and obtain a single magnetic-sublattice (Cu-sublattice). As mentioned in the main manuscript, this helps in exploring the various spin arrangements at only the 4a Wyckoff position occupied by Cu atoms, namely A-type, C-type and G-type. Since 4a Wyckoff position is *fully compatible* with altermagnetism, all three spin arrangements lead to the altermagnetic phase. The following subsections reveal this in more detail.

1. *A-type*

The spin splitting as a consequence of A-type spin arrangement in $CuGaPO_5$ has been shown along specific momentum directions in the main manuscript. Here, in Fig. S1 we show the spin splitting, as well as spin-degeneracy, along all other momentum directions (body-diagonals and different k_i planes) as a consequence of the spin space group (SSG) symmetries given by Eqs.(1) and (4) of main manuscript.

2. *C-type*

The spin splitting as a consequence of C-type spin arrangement in $CuGaPO_5$ has been shown along specific momentum directions in the main manuscript. Here, in Fig. S2 we show the spin splitting, as well as spin-degeneracy, along all other momentum directions (body-diagonals and different k_i planes) as a consequence of the spin space group (SSG) symmetries given by Eqs.(1) and (7) of main manuscript.

3. *G-type*

The spin splitting as a consequence of G-type spin arrangement in $CuGaPO_5$ has been shown along specific momentum directions in the main manuscript. Here, in Fig. S3 we show the spin splitting, as well as spin-degeneracy, along all other momentum directions (body-diagonals and different k_i planes) as a consequence of the spin space group (SSG) symmetries given by Eqs.(1) and (10) of main manuscript.

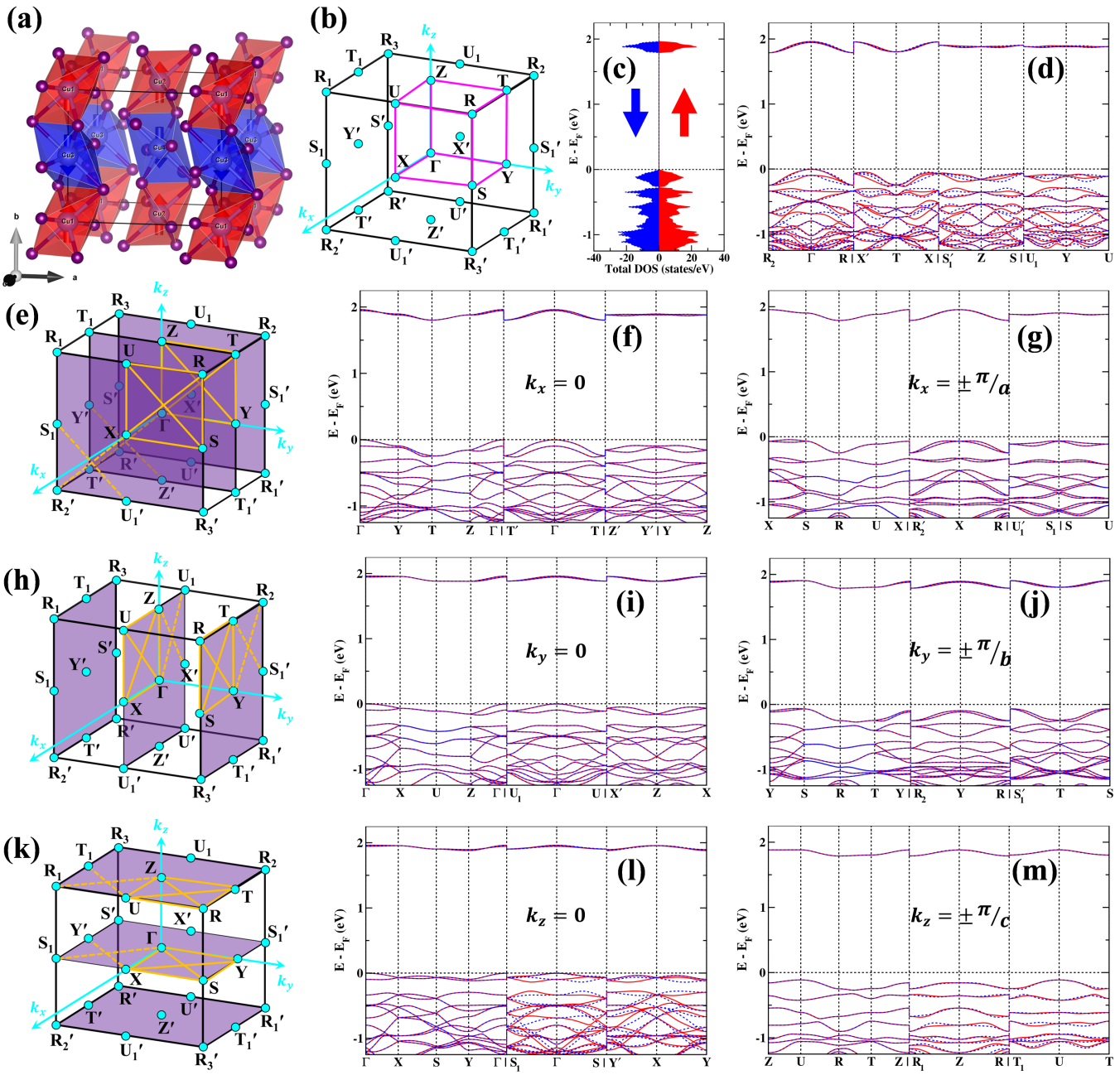

FIG. S1. (a) The Cu sublattice with A-type spin arrangement. The red octahedra denote the up-spin sublattice and the blue octahedra denote the down-spin sublattice. (b) *Primitive* orthorhombic Brillouin zone (BZ) with the high-symmetry points shown as cyan dots and the irreducible Brillouin zone (IBZ) marked by magenta lines. (c) Spin-polarized electronic total density of states (DOS) of $CuGaPO_5$. (d) Spin-polarized electronic band structure of $CuGaPO_5$ along body diagonals of the IBZ showing spin-splitting. (e) BZ with the $k_x = 0$ and $k_x = \pm\frac{\pi}{a}$ planes highlighted in purple. The high-symmetry directions on the respective planes have been highlighted by orange lines and the spin-polarized electronic band structures of $CuGaPO_5$ along these lines have been shown in (f) and (g). (h-j) The same for $k_y = 0$ and $k_y = \pm\frac{\pi}{b}$ planes. (k-m) The same for $k_z = 0$ and $k_z = \pm\frac{\pi}{c}$ planes. In (e), (h) and (k), the solid orange lines denote paths within the IBZ while the broken orange lines denote paths outside the IBZ.

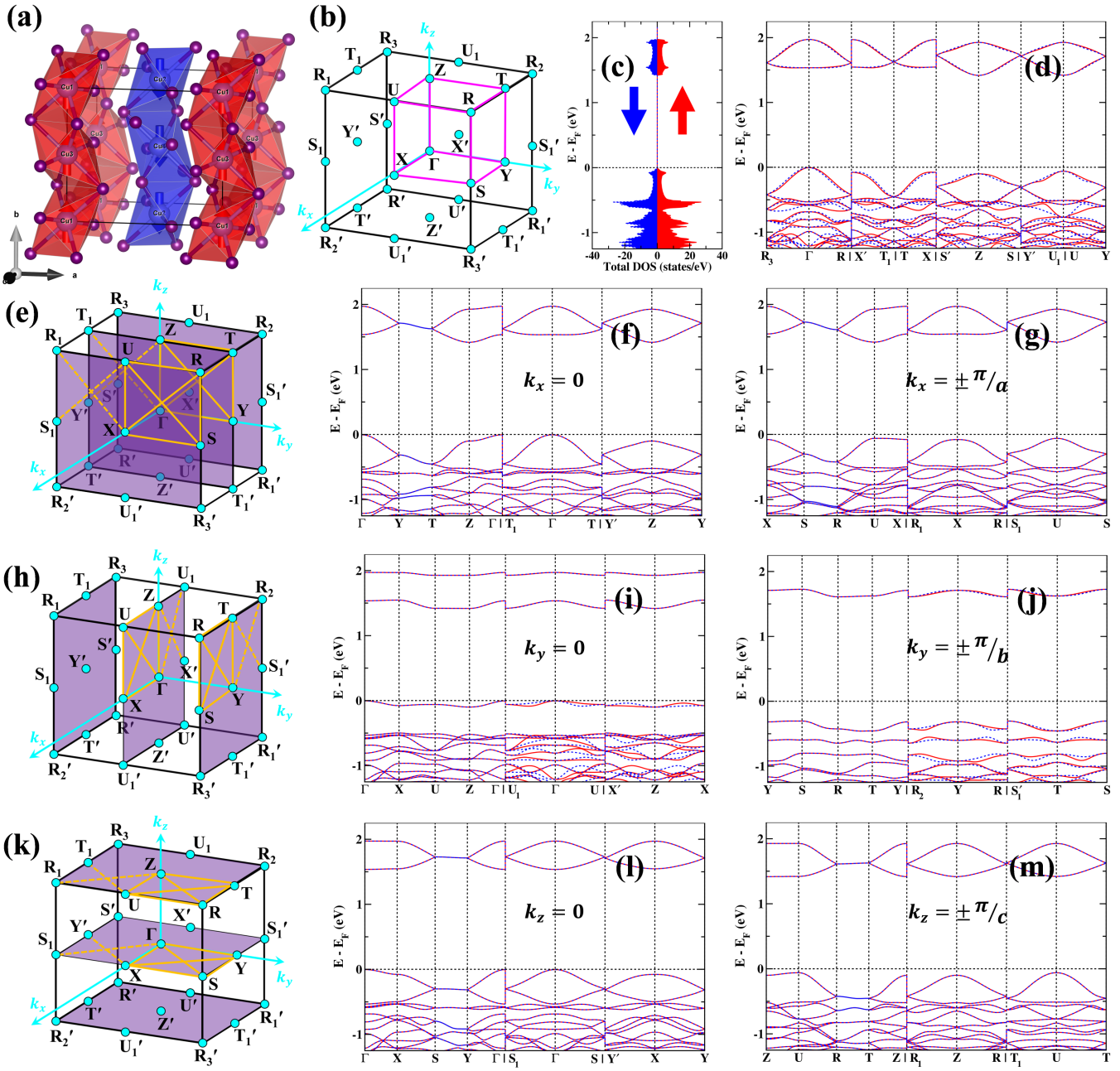

FIG. S2. (a) The Cu sublattice with C-type spin arrangement. The red octahedra denote the up-spin sublattice and the blue octahedra denote the down-spin sublattice. (b) *Primitive* orthorhombic Brillouin zone (BZ) with the high-symmetry points shown as cyan dots and the irreducible Brillouin zone (IBZ) marked by magenta lines. (c) Spin-polarized electronic total density of states (DOS) of $CuGaPO_5$. (d) Spin-polarized electronic band structure of $CuGaPO_5$ along body diagonals of the IBZ showing spin-splitting. (e) BZ with the $k_x = 0$ and $k_x = \pm\frac{\pi}{a}$ planes highlighted in purple. The high-symmetry directions on the respective planes have been highlighted by orange lines and the spin-polarized electronic band structures of $CuGaPO_5$ along these lines have been shown in (f) and (g). (h-j) The same for $k_y = 0$ and $k_y = \pm\frac{\pi}{b}$ planes. (k-m) The same for $k_z = 0$ and $k_z = \pm\frac{\pi}{c}$ planes. In (e), (h) and (k), the solid orange lines denote paths within the IBZ while the broken orange lines denote paths outside the IBZ.

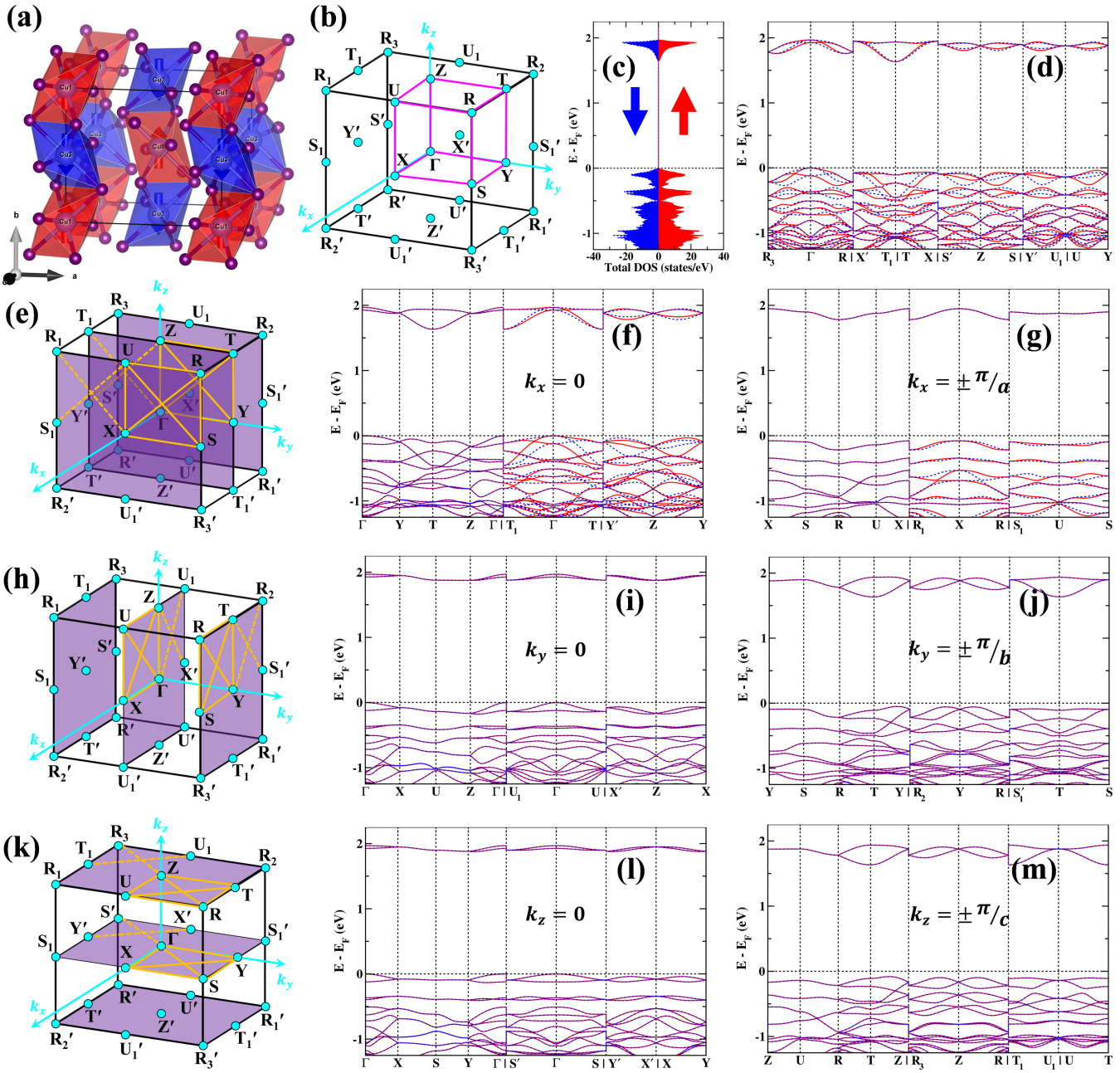

FIG. S3. (a) The Cu sublattice with G-type spin arrangement. The red octahedra denote the up-spin sublattice and the blue octahedra denote the down-spin sublattice. (b) *Primitive* orthorhombic Brillouin zone (BZ) with the high-symmetry points shown as cyan dots and the irreducible Brillouin zone (IBZ) marked by magenta lines. (c) Spin-polarized electronic total density of states (DOS) of $CuGaPO_5$. (d) Spin-polarized electronic band structure of $CuGaPO_5$ along body diagonals of the IBZ showing spin-splitting. (e) BZ with the $k_x = 0$ and $k_x = \pm\frac{\pi}{a}$ planes highlighted in purple. The high-symmetry directions on the respective planes have been highlighted by orange lines and the spin-polarized electronic band structures of $CuGaPO_5$ along these lines have been shown in (f) and (g). (h-j) The same for $k_y = 0$ and $k_y = \pm\frac{\pi}{b}$ planes. (k-m) The same for $k_z = 0$ and $k_z = \pm\frac{\pi}{c}$ planes. In (e), (h) and (k), the solid orange lines denote paths within the IBZ while the broken orange lines denote paths outside the IBZ.

B. $CaFePO_5$

The hypothetical compound $CaFePO_5$ by replacing Cu with Ca so as to maintain charge neutrality and obtain a single magnetic-sublattice (Fe-sublattice). As mentioned in the main manuscript, this helps in exploring the various spin arrangements at only the 4c Wyckoff position occupied by Fe atoms, namely $(+-+-)$-type, $(+--+)$-type and $(++--)$-type. Since 4c Wyckoff position is *partially compatible* with altermagnetism, only the $(+-+-)$-type spin arrangement leads to the altermagnetic phase whereas the other spin arrangements yield antiferromagnetic phase. The following subsections reveal this in more detail.

1. (+−+−)-type

The spin splitting as a consequence of $(+-+-)$-type spin arrangement in $CaFePO_5$ has been shown along specific momentum directions in the main manuscript. Here, in Fig. S4 we show the spin splitting, as well as spin-degeneracy, along all other momentum directions (body-diagonals and different k_i planes) as a consequence of the SSG symmetries given by Eqs.(1) and (7) of main manuscript.

2. (++−−)-type

The spin-degeneracy as a consequence of $(++--)$-type spin arrangement in $CaFePO_5$ has been shown along specific momentum directions in the main manuscript. Here, in Fig. S5 we show the spin-degeneracy, along all other momentum directions (body-diagonals and different k_i planes) as a consequence of the SSG symmetries given by Eqs.(1) and (11) of main manuscript.

3. (+−−+)-type

The spin-degeneracy as a consequence of $(+--+)$-type spin arrangement in $CaFePO_5$ has been shown along specific momentum directions in the main manuscript. Here, in Fig. S6 we show the spin-degeneracy, along all other momentum directions (body-diagonals and different k_i planes) as a consequence of the SSG symmetries given by Eqs.(1) and (11) of main manuscript.

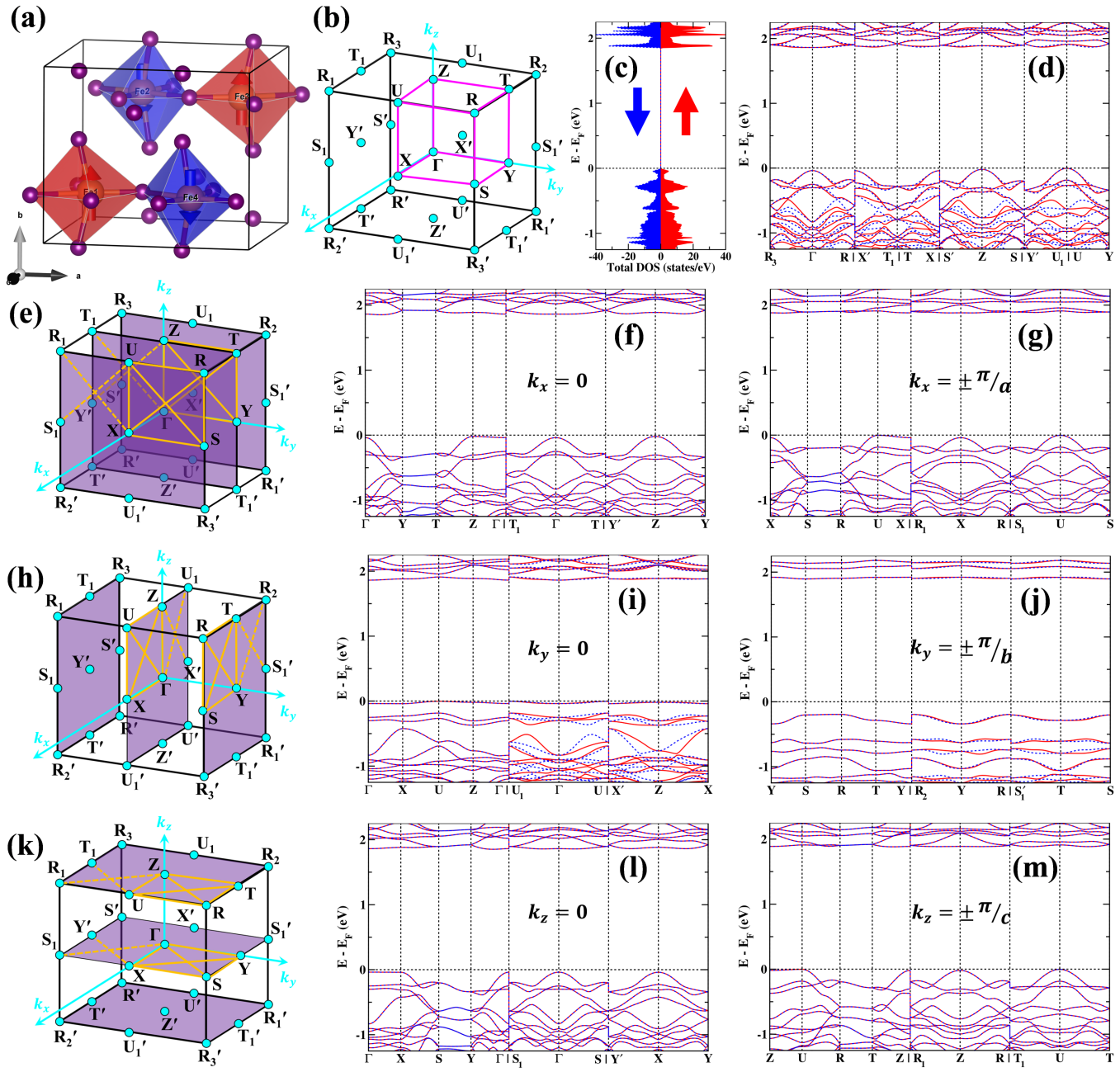

FIG. S4. (a) The Fe sublattice with $(+-+-)$-type spin arrangement. The red octahedra denote the up-spin sublattice and the blue octahedra denote the down-spin sublattice. (b) *Primitive* orthorhombic Brillouin zone (BZ) with the high-symmetry points shown as cyan dots and the irreducible Brillouin zone (IBZ) marked by magenta lines. (c) Spin-polarized electronic total density of states (DOS) of $CaFePO_5$. (d) Spin-polarized electronic band structure of $CaFePO_5$ along body diagonals of the IBZ showing spin-splitting, characteristic of the altermagnetic phase. (e) BZ with the $k_x = 0$ and $k_x = \pm\frac{\pi}{a}$ planes highlighted in purple. The high-symmetry directions on the respective planes have been highlighted by orange lines and the spin-polarized electronic band structures of $CaFePO_5$ along these lines have been shown in (f) and (g). (h-j) The same for $k_y = 0$ and $k_y = \pm\frac{\pi}{b}$ planes. (k-m) The same for $k_z = 0$ and $k_z = \pm\frac{\pi}{c}$ planes. In (e), (h) and (k), the solid orange lines denote paths within the IBZ while the broken orange lines denote paths outside the IBZ.

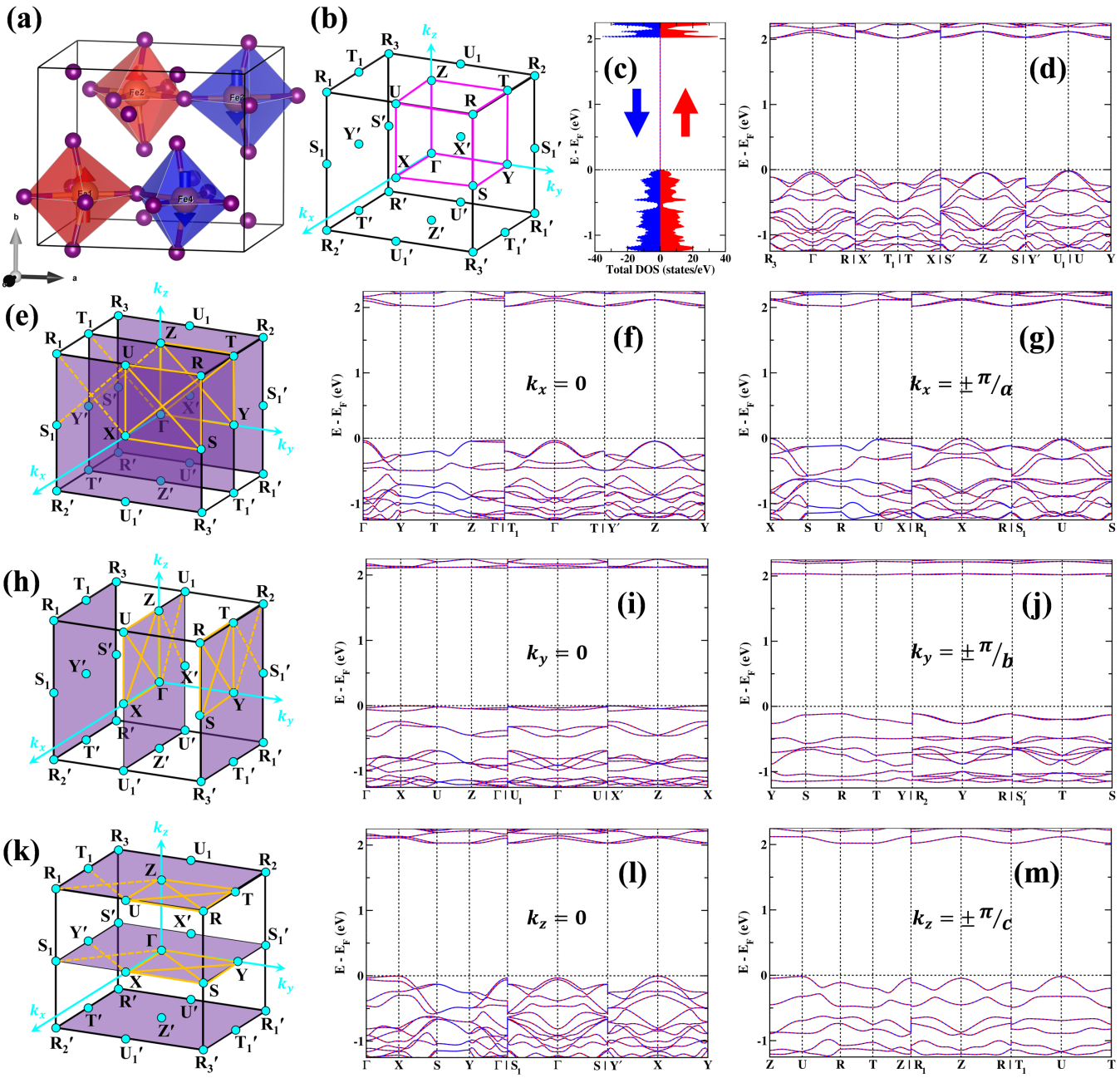

FIG. S5. (a) The Fe sublattice with (++−−)-type spin arrangement. The red octahedra denote the up-spin sublattice and the blue octahedra denote the down-spin sublattice. (b) *Primitive* orthorhombic Brillouin zone (BZ) with the high-symmetry points shown as cyan dots and the irreducible Brillouin zone (IBZ) marked by magenta lines. (c) Spin-polarized electronic total density of states (DOS) of $CaFePO_5$. (d) Spin-polarized electronic band structure of $CaFePO_5$ along body diagonals of the IBZ showing spin-degeneracy, characteristic of the antiferromagnetic phase. (e) BZ with the $k_x = 0$ and $k_x = \pm\frac{\pi}{a}$ planes highlighted in purple. The high-symmetry directions on the respective planes have been highlighted by orange lines and the spin-polarized electronic band structures of $CaFePO_5$ along these lines have been shown in (f) and (g). (h-j) The same for $k_y = 0$ and $k_y = \pm\frac{\pi}{b}$ planes. (k-m) The same for $k_z = 0$ and $k_z = \pm\frac{\pi}{c}$ planes. In (e), (h) and (k), the solid orange lines denote paths within the IBZ while the broken orange lines denote paths outside the IBZ.

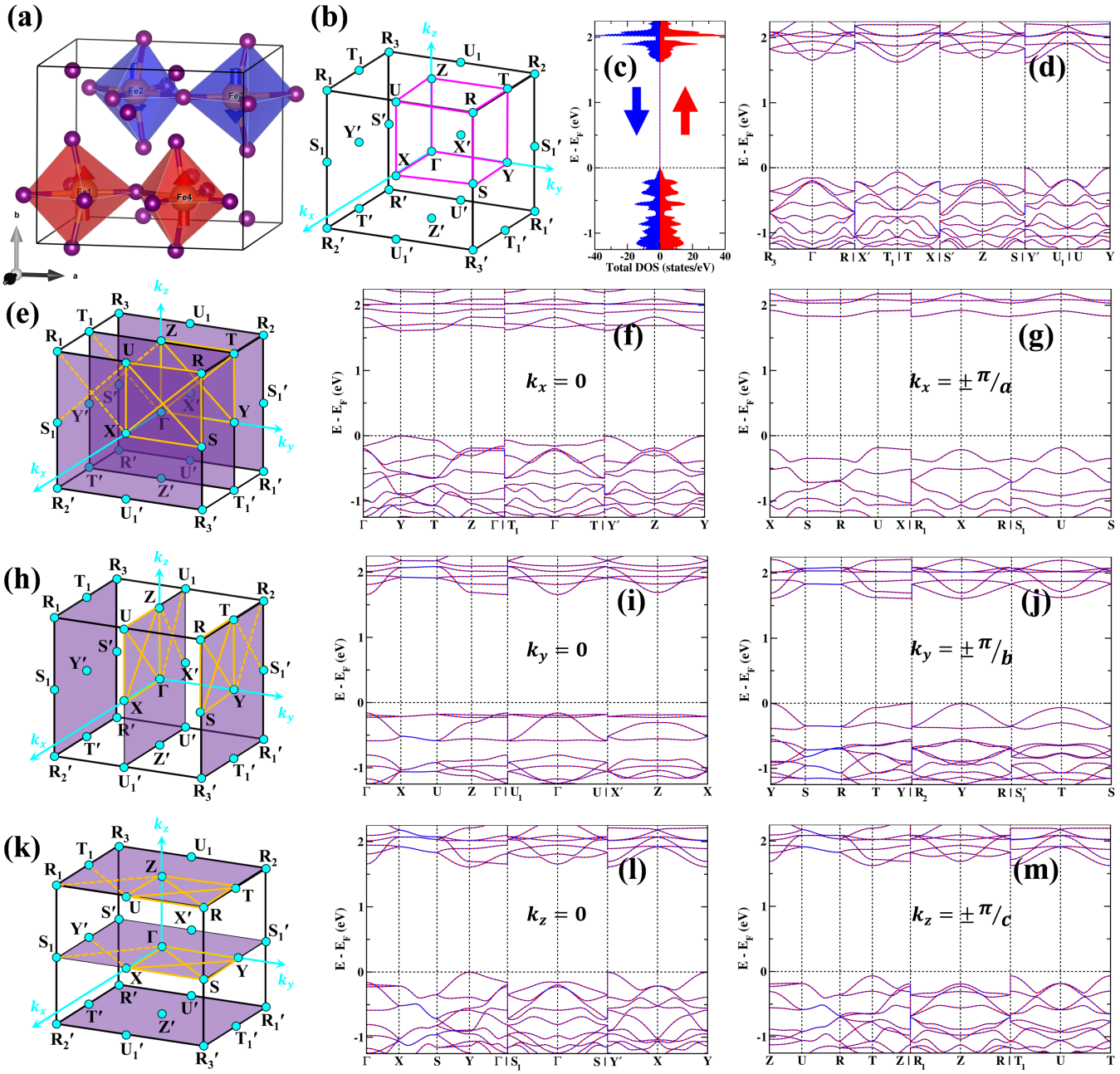

FIG. S6. (a) The Fe sublattice with $(+--+)$-type spin arrangement. The red octahedra denote the up-spin sublattice and the blue octahedra denote the down-spin sublattice. (b) *Primitive* orthorhombic Brillouin zone (BZ) with the high-symmetry points shown as cyan dots and the irreducible Brillouin zone (IBZ) marked by magenta lines. (c) Spin-polarized electronic total density of states (DOS) of $CaFePO_5$. (d) Spin-polarized electronic band structure of $CaFePO_5$ along body diagonals of the IBZ showing spin-degeneracy, characteristic of the antiferromagnetic phase. (e) BZ with the $k_x = 0$ and $k_x = \pm\frac{\pi}{a}$ planes highlighted in purple. The high-symmetry directions on the respective planes have been highlighted by orange lines and the spin-polarized electronic band structures of $CaFePO_5$ along these lines have been shown in (f) and (g). (h-j) The same for $k_y = 0$ and $k_y = \pm\frac{\pi}{b}$ planes. (k-m) The same for $k_z = 0$ and $k_z = \pm\frac{\pi}{c}$ planes. In (e), (h) and (k), the solid orange lines denote paths within the IBZ while the broken orange lines denote paths outside the IBZ.

SIV. ALTERFERRIMAGNETS

A. Magnetic configurations of $CuFePO_5$

In the main text, it has been mentioned that there are nine possible magnetic configurations corresponding to different spin arrangements in $CuFePO_5$ at the 4a and 4c Wyckoff positions. These have been tabulated here.

TABLE S1. Ground state energy of possible magnetic configurations of $CuFePO_5$ in the absence of SOC.

Spin arrangement of Cu sublattice	Spin arrangement of Fe sublattice	Relative ground state energy per atom (meV)	Maximum spin-splitting (meV)
A		8.37	153.10
C	+−+−	0.00	173.00
G		8.39	144.10
A		7.17	89.10
C	++−−	7.68	118.30
G		7.18	177.90
A		14.11	121.20
C	+−−+	14.57	74.70
G		14.13	146.70

The magnetic ground state of $CuFePO_5$ is in good agreement with earlier neutron diffraction studies [12–14] where the Cu sublattice adopts a collinear C-type spin arrangement and the Fe sublattice exhibits a collinear (+−+−)-type spin arrangement.

B. (+−+−)-type spin arrangement at 4c Wyckoff position

All three different magnetic configurations (C-, A-, G-type) of Cu sublattice at 4a Wyckoff position corresponding to the fixed (+−+−)-type spin arrangement of Fe sublattice at the 4c Wyckoff position have been discussed in some detail in Sec. III of main manuscript. Here, we further showcase the electronic structure of these Alterferrimagnets along all possible high symmetry directions and planes in the Brillouin zone.

1. *C-type spin arrangement at 4a Wyckoff position*

Figure S7(a) displays C-type spin arrangement of Cu sublattice and (+−+−)-type spin arrangement of Fe sublattice in $CuFePO_5$. Such spin arrangement leads to SSG $\boldsymbol{P\bar{1}n1m\bar{1}a}$ (S62.448) [1, 4, 15] as derived in the main manuscript. Figure S7(b) shows the BZ along with the IBZ and Fig. S7(c) shows the spin-polarized total DOS. The resulting altermagnetic spin-splitting for this spin arrangement along the IBZ body diagonals is shown in Fig. S7(d). The spin-degeneracies and spin-splittings on the high symmetry planes $k_x = 0, \pm\pi/a$, $k_y = 0, \pm\pi/b$ and $k_z = 0, \pm\pi/c$, as enforced by the SSG symmetries, are displayed in Figs. S7(e–m).

2. *A-type spin arrangement at 4a Wyckoff position*

Figure S8(a) displays A-type spin arrangement of Cu sublattice and (+−+−)-type spin arrangement of Fe sublattice in $CuFePO_5$. Such spin arrangement leads to SSG $\boldsymbol{P\bar{1}2_1/\bar{1}n}$ (S14.79) [1, 4, 15] as derived in the main manuscript. Figure S8(b) shows the BZ along with the IBZ and Fig. S8(c) shows the spin-polarized total DOS. The resulting altermagnetic spin-splitting for this spin arrangement along the IBZ body diagonals is shown in Fig. S8(d). The spin-degeneracies and spin-splittings on the high symmetry planes $k_x = 0, \pm\pi/a$, $k_y = 0, \pm\pi/b$ and $k_z = 0, \pm\pi/c$, as enforced by the SSG symmetries, are displayed in Figs. S8(e–m).

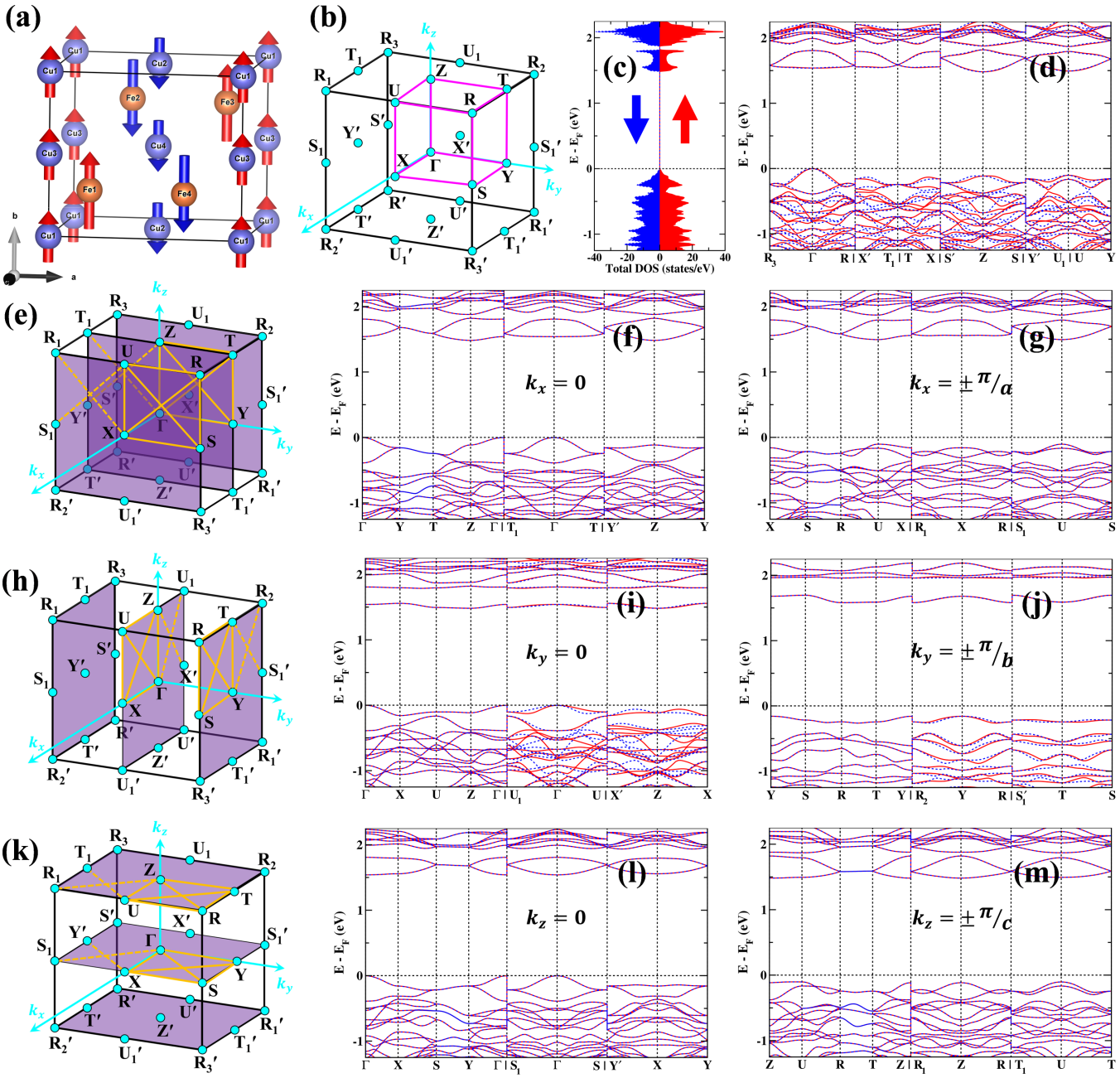

FIG. S7. The Cu and Fe sublattices with C-type and (+−+−)-type spin ordering, respectively (only magnetic atoms shown) for $CuFePO_5$. (b) Primitive orthorhombic BZ with high-symmetry points (cyan) and the irreducible BZ (IBZ, magenta). (c) Spin-polarized total density of states (DOS) of $CuFePO_5$. (d) Spin-polarized band structure along IBZ body diagonals, showing spin splitting characteristic of the altermagnetic phase. (e) BZ highlighting the $k_x = 0, \pm\frac{\pi}{a}$ planes (purple); corresponding band structures along indicated high-symmetry lines are shown in (f,g). (h–j) Same for $k_y = 0, \pm\frac{\pi}{b}$. (k–m) Same for $k_z = 0, \pm\frac{\pi}{c}$. In (e), (h), and (k), solid (dashed) orange lines denote paths inside (outside) the IBZ.

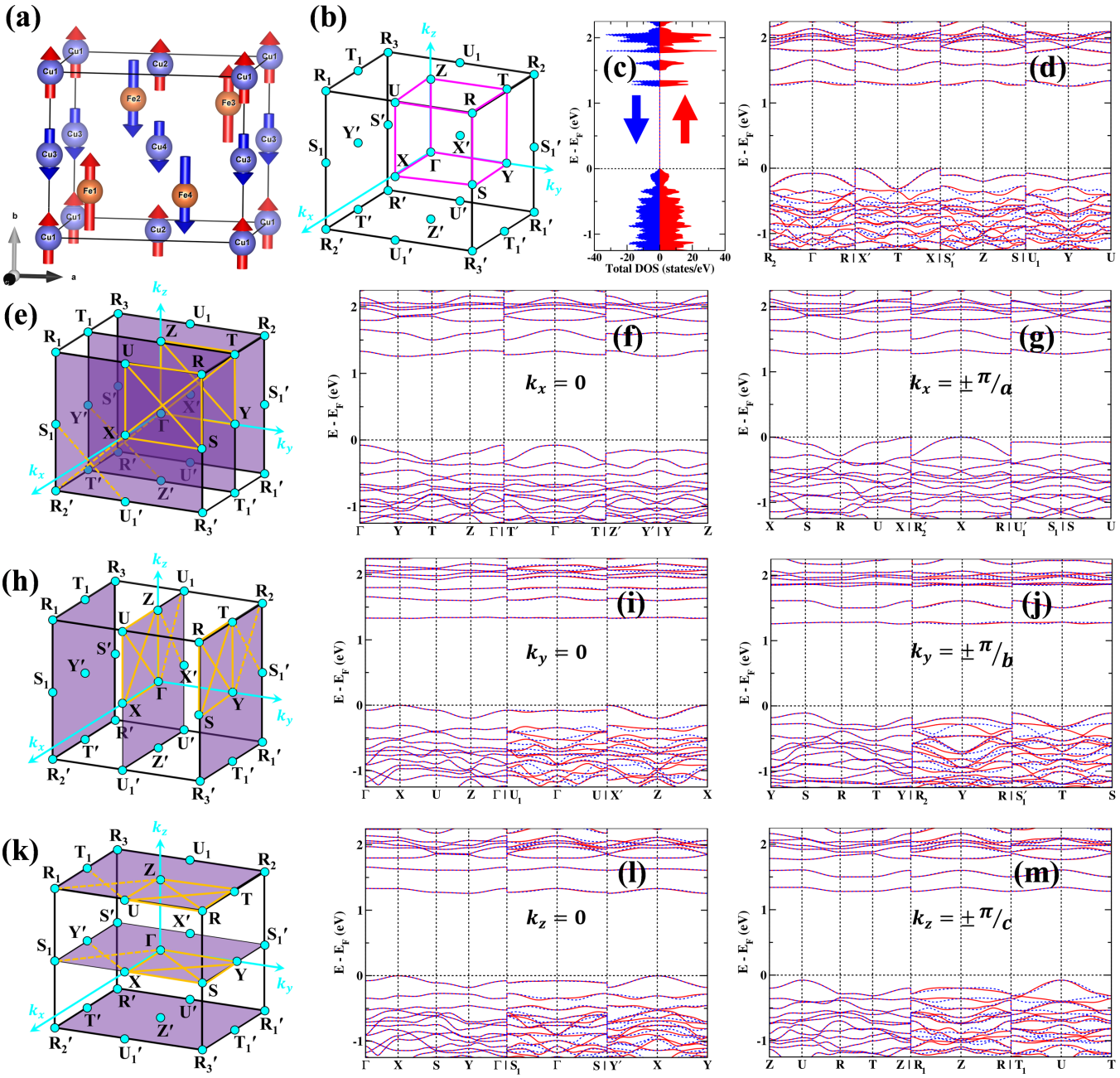

FIG. S8. The Cu and Fe sublattices with A-type and (+−+−)-type spin ordering, respectively (only magnetic atoms shown) for $CuFePO_5$. (b) Primitive orthorhombic BZ with high-symmetry points (cyan) and the irreducible BZ (IBZ, magenta). (c) Spin-polarized total density of states (DOS). (d) Spin-polarized band structure along IBZ body diagonals, showing spin splitting characteristic of the altermagnetic phase. (e) BZ highlighting the $k_x = 0, \pm\frac{\pi}{a}$ planes (purple); corresponding band structures along indicated high-symmetry lines are shown in (f,g). (h–j) Same for $k_y = 0, \pm\frac{\pi}{b}$. (k–m) Same for $k_z = 0, \pm\frac{\pi}{c}$. In (e), (h), and (k), solid (dashed) orange lines denote paths inside (outside) the IBZ.

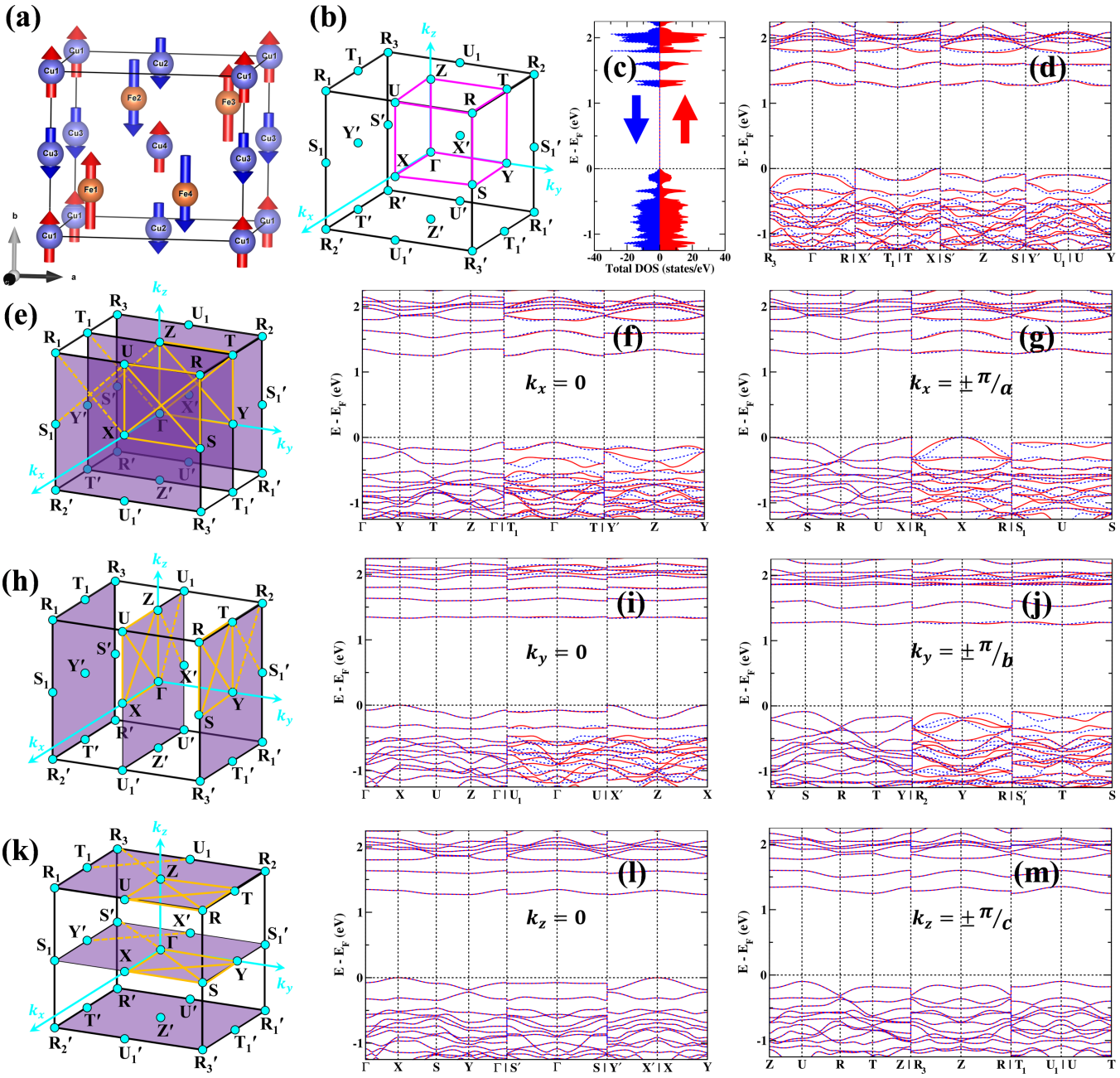

FIG. S9. The Cu and Fe sublattices with G-type and $(+-+-)$-type spin ordering, respectively (only magnetic atoms shown) for $CuFePO_5$. (b) Primitive orthorhombic BZ with high-symmetry points (cyan) and the irreducible BZ (IBZ, magenta). (c) Spin-polarized total density of states (DOS). (d) Spin-polarized band structure along IBZ body diagonals, showing spin splitting characteristic of the altermagnetic phase. (e) BZ highlighting the $k_x = 0, \pm\frac{\pi}{a}$ planes (purple); corresponding band structures along indicated high-symmetry lines are shown in (f,g). (h–j) Same for $k_y = 0, \pm\frac{\pi}{b}$. (k–m) Same for $k_z = 0, \pm\frac{\pi}{c}$. In (e), (h), and (k), solid (dashed) orange lines denote paths inside (outside) the IBZ.

3. G-type spin arrangement at 4a Wyckoff position

Figure S9(a) displays G-type spin arrangement of Cu sublattice and $(+-+-)$-type spin arrangement of Fe sublattice in $CuFePO_5$. Such spin arrangement leads to SSG $\boldsymbol{P^{\bar{1}}2_1/^{\bar{1}}a}$ (S14.79) [1, 4, 15] as derived in the main manuscript. Figure S9(b) shows the BZ along with the IBZ and Fig. S9(c) shows the spin-polarized total DOS. The resulting altermagnetic spin-splitting for this spin arrangement along the IBZ body diagonals is shown in Fig. S9(d). The spin-degeneracies and spin-splittings on the high symmetry planes $k_x = 0, \pm\pi/a$, $k_y = 0, \pm\pi/b$ and $k_z = 0, \pm\pi/c$, as enforced by the SSG symmetries, are displayed in Figs. S9(e–m).

SV. ALTERFERRIMAGNETS WITH SYMMETRIES OF ALTERMAGNETS

In the main text, it has been mentioned that there are nine possible magnetic configurations corresponding to different spin arrangements in $CuFePO_5$ at the 4a and 4c Wyckoff positions (see Table I of main manuscript), and all three configurations corresponding to the $(+-+-)$-type spin arrangement at the 4c Wyckoff position have been discussed in detail (see Sec. III of main manuscript). Now, the remaining six configurations shall be discussed here. Since the Wyckoff postion 4c is *partially compatible* with the AM phase, these remaining configurations also give rise to alterferrimagnetic states with lower crystallographic symmetry in the non-trivial spin group $\mathbb{G}_{\mathbf{S}}$, as discussed in Sec. IIID of main manuscript, mostly determined by the spin arrangement at the *fully compatible* Wyckoff position 4a. Interestingly, the alterferrimagnetic states discussed here show spin-splitting similar to that of the pure altermagnetic states discussed in Sec. IIIA of main manuscript. This is a consequence of the symmetries of the spin only group $\mathfrak{G}_{\mathbf{S}}$ which gives rise to additional spin-degeneracies when the full SSG $\mathcal{G}$ of these alterferrimagnetic states is taken into account.

A. $(++--)$-type spin arrangement at 4c Wyckoff position

The $(++--)$-type spin arrangement at the 4c Wyckoff position yields the AFM phase and hence the Fe sublattice in $CuFePO_5$ is expected to show spin-degeneracy throughout the Brillouin zone (also see Sec. IIIB 2 of main manuscript). Then the three possible spin arrangements of the Cu sublattice at the 4a Wyckoff position gives rise to SSG symmetries similar to those discussed in Sec. IIIA of main manuscript.

1. *A-type spin arrangement at 4a Wyckoff position*

Figure S10(a) displays A-type spin arrangement of Cu sublattice and $(++--)$-type spin arrangement of Fe sublattice in $CuFePO_5$. From the parent crystallographic space group $\mathbf{G} = \boldsymbol{Pnma}$, the same-spin sublattice transformations for A-type spin arrangement at the 4a Wyckoff position and $(++--)$-type spin arrangement at the 4c Wyckoff position form the *halving* subgroups $\mathbf{H_1} = \tilde{\boldsymbol{C}}^{\boldsymbol{z}}_{\boldsymbol{2h}}$ and $\mathbf{H_4} = \tilde{\boldsymbol{C}}^{\boldsymbol{z}}_{\boldsymbol{2v}}$ respectively (derived and discussed in Secs. IIIA 1 and IIIB 2 of main manuscript). The cosets $\mathbf{G} - \mathbf{H_1}$ and $\mathbf{G} - \mathbf{H_4}$ provide the respective opposite-spin sublattice transformations. Then, the *common* same-spin and opposite-spin sublattice transformations are $\mathbf{H_1} \cap \mathbf{H_4} = \{\mathbb{I}, \tilde{C}_{2z}\}$ and $(\mathbf{G} - \mathbf{H_1}) \cap (\mathbf{G} - \mathbf{H_4}) = \{\tilde{C}_{2y}, \tilde{C}_{2x}\}$ respectively. Then the reduced crystallographic space group is given by $\tilde{\boldsymbol{D}}_{\mathbf{2}} = \{\mathbb{I}, \tilde{C}_{2z}, \tilde{C}_{2y}, \tilde{C}_{2x}\}$, *isomorphic* to $\boldsymbol{P2_12_12_1}$ $(\boldsymbol{D}^{\mathbf{4}}_{\mathbf{2}})$ [1, 2] and a subgroup of $\mathbf{G}$. The non-trivial spin group becomes:

$$\mathbb{G}_{\mathbf{S}} = \widetilde{\boldsymbol{\mathcal{S}}} \otimes \tilde{\boldsymbol{D}}_{\mathbf{2}} = [\,\mathfrak{I} \,||\, \{\mathbb{I}, \tilde{C}_{2z}\}\,] \cup [\,\mathfrak{C}_2 \,||\, \{\tilde{C}_{2y}, \tilde{C}_{2x}\}\,] \tag{S.4}$$

Thus, A-type spin arrangement on the Cu sublattice and $(++--)$-type spin arrangement on the Fe sublattice in $CuFePO_5$ leads to SSG $\boldsymbol{P\bar{1}2_1\bar{1}2_11^{\prime}2_1}$ (19.27) [4, 15]. From Eqs. (1), (4) and (11) of main manuscript and eq. (S.4), all the resulting spin-degenerate nodal lines and nodal planes across the BZ can be systematically mapped out using the *isomorphic* spin point groups, as discussed in Sec. III of main manuscript. Figure S10(b) shows the BZ along with the IBZ. First-principles calculations reveal fully compensated nature of both Cu and Fe sublattices which is evident from the spin-polarized total DOS as shown in Fig. S10(c). The resulting altermagnetic spin-splitting for these spin arrangements along the IBZ body diagonals is shown in Figure S10(d). The spin-degeneracies and splittings on the high symmetry planes $k_x = 0, \pm\pi/a$, $k_y = 0, \pm\pi/b$ and $k_z = 0, \pm\pi/c$, as enforced by the SSG symmetries, are displayed in Figs. S10(e–m).

2. *C-type spin arrangement at 4a Wyckoff position*

Figure S11(a) displays C-type spin arrangement of Cu sublattice and $(++--)$-type spin arrangement of Fe sublattice in $CuFePO_5$. From the parent crystallographic space group $\mathbf{G} = \boldsymbol{Pnma}$, the same-spin sublattice transformations for A-type spin arrangement at the 4a Wyckoff position and $(++--)$-type spin arrangement at the 4c Wyckoff position form the *halving* subgroups $\mathbf{H_2} = \tilde{\boldsymbol{C}}^{\boldsymbol{y}}_{\boldsymbol{2h}}$ and $\mathbf{H_4} = \tilde{\boldsymbol{C}}^{\boldsymbol{z}}_{\boldsymbol{2v}}$ respectively (derived and discussed in Secs. IIIA 2 and IIIB 2 of main manuscript). The cosets $\mathbf{G} - \mathbf{H_2}$ and $\mathbf{G} - \mathbf{H_4}$ provide the respective opposite-spin sublattice transformations. Then, the *common* same-spin and opposite-spin sublattice transformations are $\mathbf{H_2} \cap \mathbf{H_4} = \{\mathbb{I}, \tilde{m}_{zx}\}$ and $(\mathbf{G} - \mathbf{H_2}) \cap (\mathbf{G} - \mathbf{H_4}) = \{\tilde{m}_{xy}, \tilde{C}_{2x}\}$ respectively. Then the reduced crystallographic space group is given by

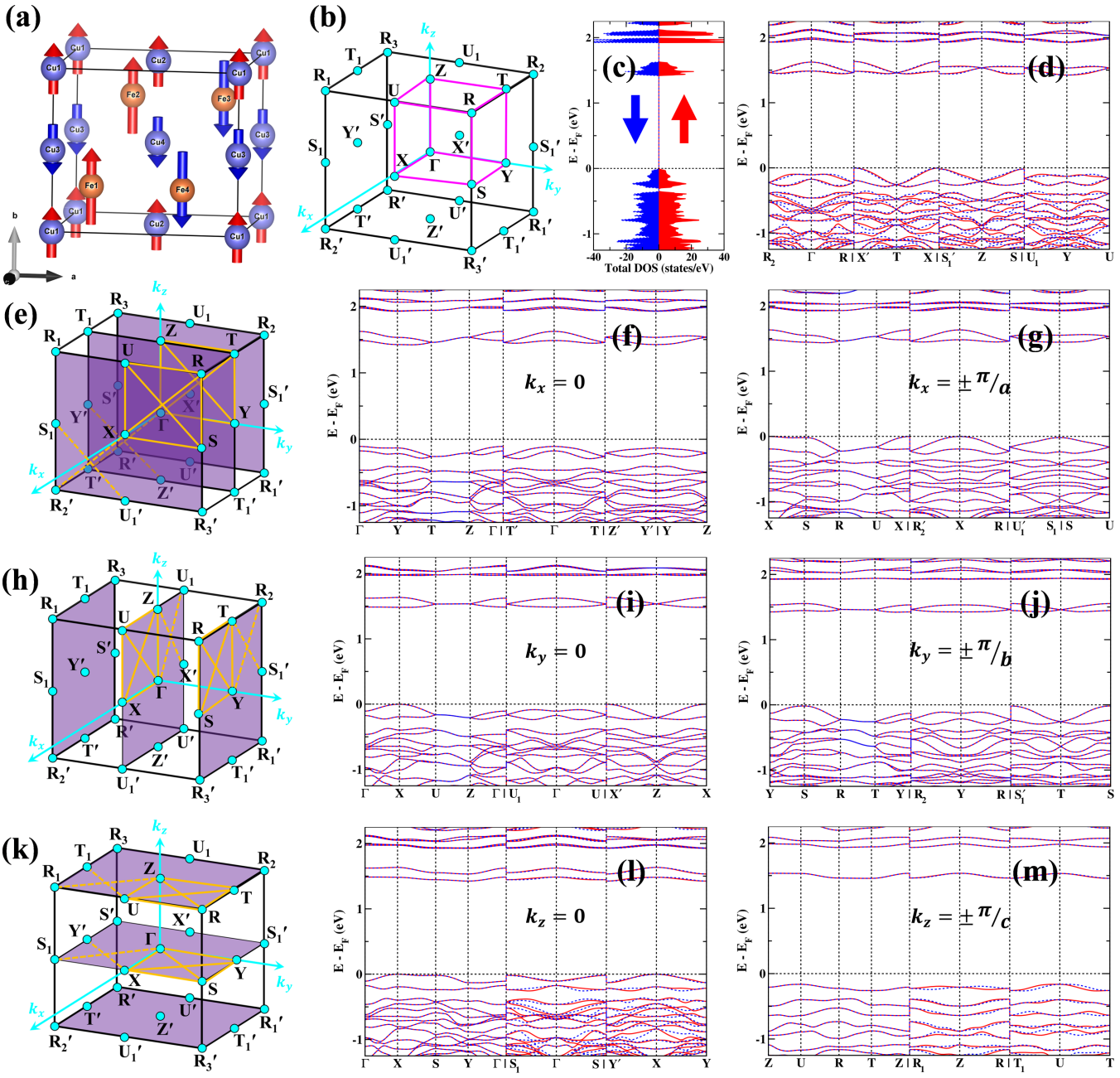

FIG. S10. (a) The Cu and Fe sublattices with A-type and Fe(++−−)-type spin arrangement respectively. Only the magnetic atoms are shown for visual clarity. (b) *Primitive* orthorhombic Brillouin zone (BZ) with the high-symmetry points shown as cyan dots and the irreducible Brillouin zone (IBZ) marked by magenta lines. (c) Spin-polarized electronic total density of states (TDOS) of $CuFePO_5$. (d) Spin-polarized electronic band structure of $CuFePO_5$ along body diagonals of the IBZ showing spin-splitting, characteristic of the altermagnetic phase. (e) BZ with the $k_x = 0$ and $k_x = \pm\frac{\pi}{a}$ planes highlighted in purple. The high-symmetry directions on the respective planes have been highlighted by orange lines and the spin-polarized electronic band structures of $CuFePO_5$ along these lines have been shown in (f) and (g). (h-j) The same for $k_y = 0$ and $k_y = \pm\frac{\pi}{b}$ planes. (k-m) The same for $k_z = 0$ and $k_z = \pm\frac{\pi}{c}$ planes. In (e), (h) and (k), the solid orange lines denote paths within the IBZ while the broken orange lines denote paths outside the IBZ.

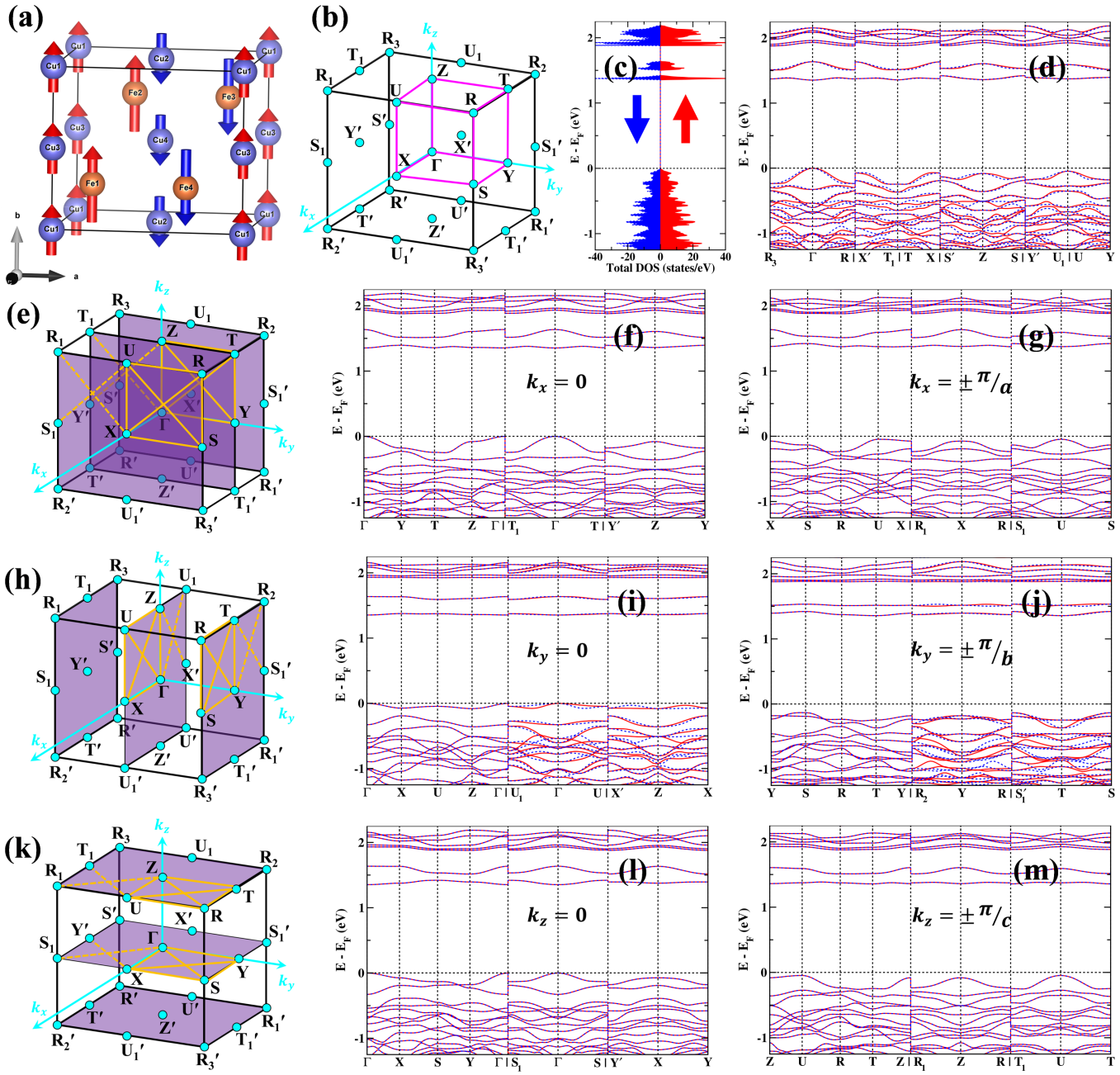

FIG. S11. (a) The Cu and Fe sublattices with C-type and Fe(++−−)-type spin arrangement respectively. Only the magnetic atoms are shown for visual clarity. (b) *Primitive* orthorhombic Brillouin zone (BZ) with the high-symmetry points shown as cyan dots and the irreducible Brillouin zone (IBZ) marked by magenta lines. (c) Spin-polarized electronic total density of states (TDOS) of $CuFePO_5$. (d) Spin-polarized electronic band structure of $CuFePO_5$ along body diagonals of the IBZ showing spin-splitting, characteristic of the altermagnetic phase. (e) BZ with the $k_x = 0$ and $k_x = \pm\frac{\pi}{a}$ planes highlighted in purple. The high-symmetry directions on the respective planes have been highlighted by orange lines and the spin-polarized electronic band structures of $CuFePO_5$ along these lines have been shown in (f) and (g). (h-j) The same for $k_y = 0$ and $k_y = \pm\frac{\pi}{b}$ planes. (k-m) The same for $k_z = 0$ and $k_z = \pm\frac{\pi}{c}$ planes. In (e), (h) and (k), the solid orange lines denote paths within the IBZ while the broken orange lines denote paths outside the IBZ.

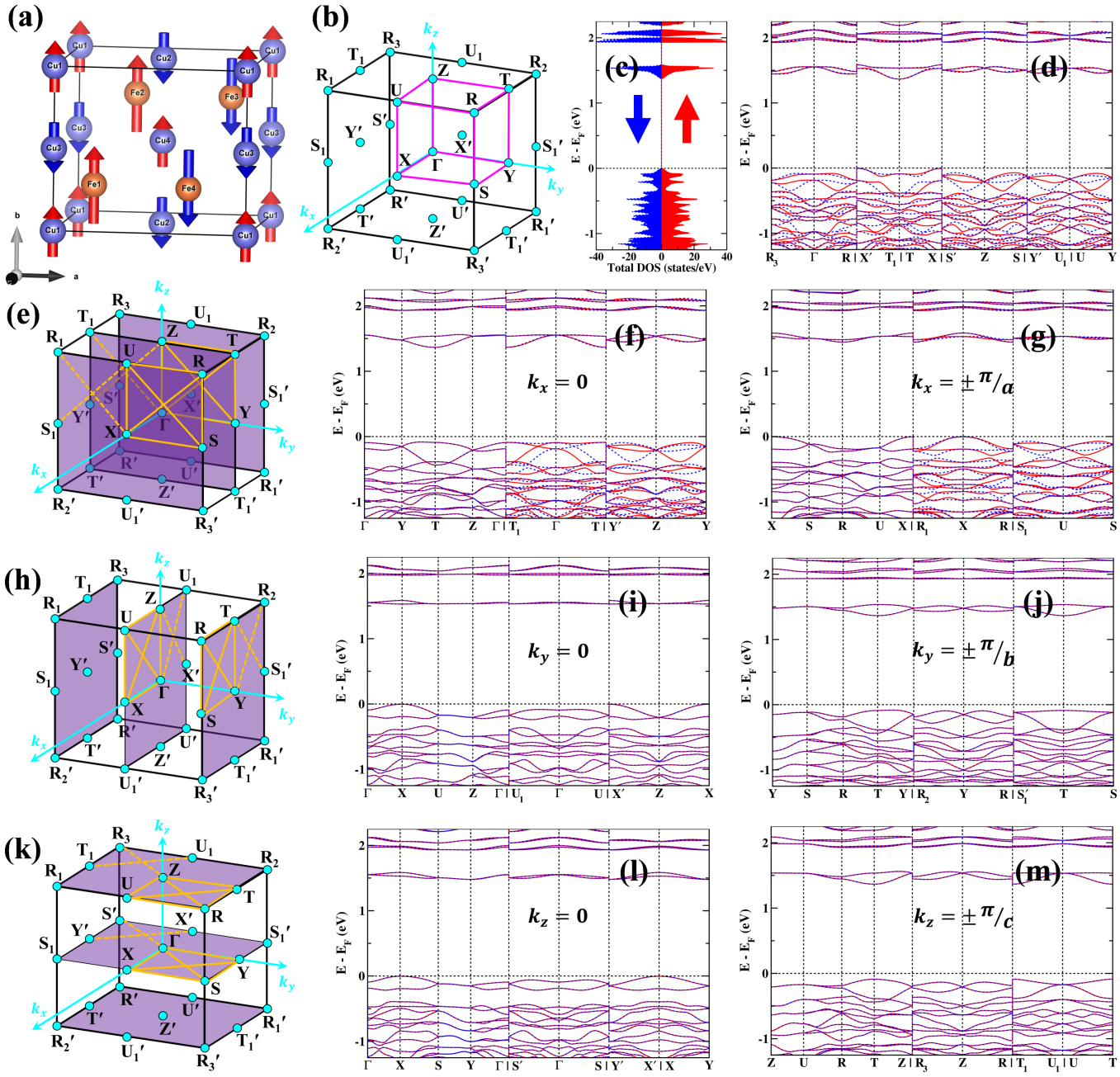

FIG. S12. (a) The Cu and Fe sublattices with G-type and Fe(++−−)-type spin arrangement respectively. Only the magnetic atoms are shown for visual clarity. (b) *Primitive* orthorhombic Brillouin zone (BZ) with the high-symmetry points shown as cyan dots and the irreducible Brillouin zone (IBZ) marked by magenta lines. (c) Spin-polarized electronic total density of states (TDOS) of $CuFePO_5$. (d) Spin-polarized electronic band structure of $CuFePO_5$ along body diagonals of the IBZ showing spin-splitting, characteristic of the altermagnetic phase. (e) BZ with the $k_x = 0$ and $k_x = \pm\frac{\pi}{a}$ planes highlighted in purple. The high-symmetry directions on the respective planes have been highlighted by orange lines and the spin-polarized electronic band structures of $CuFePO_5$ along these lines have been shown in (f) and (g). (h-j) The same for $k_y = 0$ and $k_y = \pm\frac{\pi}{b}$ planes. (k-m) The same for $k_z = 0$ and $k_z = \pm\frac{\pi}{c}$ planes. In (e), (h) and (k), the solid orange lines denote paths within the IBZ while the broken orange lines denote paths outside the IBZ.

$\tilde{\boldsymbol{C}}^{\boldsymbol{x}}_{\boldsymbol{2v}} = \{\,\mathbb{I}, \tilde{m}_{zx}, \tilde{m}_{xy}, \tilde{C}_{2x}\,\}$, *isomorphic* to $\boldsymbol{P2_1ma}$ ($\boldsymbol{C^2_{2v}}$) (also see Table I of main manuscript) [1, 2] and a subgroup of $\mathbf{G}$. The non-trivial spin group becomes:

$$\mathbb{G}_{\mathbf{S}} = \widetilde{\boldsymbol{\mathcal{S}}} \otimes \tilde{\boldsymbol{C}}^{\boldsymbol{x}}_{\boldsymbol{2v}} = [\,\mathfrak{I}\,||\,\{\,\mathbb{I}, \tilde{m}_{zx}\,\}\,] \cup [\,\mathfrak{C}_2\,||\,\{\,\tilde{m}_{xy}, \tilde{C}_{2x}\,\}\,] \tag{S.5}$$

Thus, C-type spin arrangement on the Cu sublattice and $(++--)$-type spin arrangement on the Fe sublattice in $CuFePO_5$ leads to SSG $\boldsymbol{P\,\bar{1}\,2_1\,1\,m\,\bar{1}\,a}$ (26.69) [4, 15]. From Eqs. (1), (7) and (11) of main manuscript and eq. (S.5), all the resulting spin-degenerate nodal lines and nodal planes across the BZ can be systematically mapped out using the *isomorphic* spin point groups, as discussed in Sec. III of main manuscript. Figure S11(b) shows the BZ along with the IBZ. First-principles calculations reveal fully compensated nature of both Cu and Fe sublattices which is evident from the spin-polarized total DOS as shown in Fig. S11(c). The resulting altermagnetic spin-splitting for these spin arrangements along the IBZ body diagonals is shown in Figure S11(d). The spin-degeneracies and splittings on the high symmetry planes $k_x = 0, \pm\pi/a$, $k_y = 0, \pm\pi/b$ and $k_z = 0, \pm\pi/c$, as enforced by the SSG symmetries, are displayed in Figs. S11(e–m).

3. *G-type spin arrangement at 4a Wyckoff position*

Figure S12(a) displays G-type spin arrangement of Cu sublattice and $(++--)$-type spin arrangement of Fe sublattice in $CuFePO_5$. From the parent crystallographic space group $\mathbf{G} = \boldsymbol{Pnma}$, the same-spin sublattice transformations for A-type spin arrangement at the 4a Wyckoff position and $(++--)$-type spin arrangement at the 4c Wyckoff position form the *halving* subgroups $\mathbf{H_3} = \tilde{\boldsymbol{C}}^{\boldsymbol{x}}_{\boldsymbol{2h}}$ and $\mathbf{H_4} = \tilde{\boldsymbol{C}}^{\boldsymbol{z}}_{\boldsymbol{2v}}$ respectively (derived and discussed in Secs. IIIA 3 and IIIB 2 of main manuscript). The cosets $\mathbf{G} - \mathbf{H_3}$ and $\mathbf{G} - \mathbf{H_4}$ provide the respective opposite-spin sublattice transformations. Then, the *common* same-spin and opposite-spin sublattice transformations are $\mathbf{H_3} \cap \mathbf{H_4} = \{\,\mathbb{I}, \tilde{m}_{yz}\,\}$ and $(\mathbf{G} - \mathbf{H_3}) \cap (\mathbf{G} - \mathbf{H_4}) = \{\,\tilde{m}_{xy}, \tilde{C}_{2y}\,\}$ respectively. Then the reduced crystallographic space group is given by $\tilde{\boldsymbol{C}}^{\boldsymbol{y}}_{\boldsymbol{2v}} = \{\,\mathbb{I}, \tilde{m}_{yz}, \tilde{m}_{xy}, \tilde{C}_{2y}\,\}$, *isomorphic* to $\boldsymbol{Pn2_1a}$ ($\boldsymbol{C^9_{2v}}$) (also see Table I of main manuscript) [1, 2] and a subgroup of $\mathbf{G}$. The non-trivial spin group becomes:

$$\mathbb{G}_{\mathbf{S}} = \widetilde{\boldsymbol{\mathcal{S}}} \otimes \tilde{\boldsymbol{C}}^{\boldsymbol{y}}_{\boldsymbol{2v}} = [\,\mathfrak{I}\,||\,\{\,\mathbb{I}, \tilde{m}_{yz}\,\}\,] \cup [\,\mathfrak{C}_2\,||\,\{\,\tilde{m}_{xy}, \tilde{C}_{2y}\,\}\,] \tag{S.6}$$

Thus, G-type spin arrangement on the Cu sublattice and $(++--)$-type spin arrangement on the Fe sublattice in $CuFePO_5$ leads to SSG $\boldsymbol{P\,1\,n\,\bar{1}\,2_1\,\bar{1}\,a}$ (33.147) [4, 15]. From Eqs. (1), (10) and (11) of main manuscript and eq. (S.6), all the resulting spin-degenerate nodal lines and nodal planes across the BZ can be systematically mapped out using the *isomorphic* spin point groups, as discussed in Sec. III of main manuscript. Figure S12(b) shows the BZ along with the IBZ. First-principles calculations reveal fully compensated nature of both Cu and Fe sublattices which is evident from the spin-polarized total DOS as shown in Fig. S12(c). The resulting altermagnetic spin-splitting for these spin arrangements along the IBZ body diagonals is shown in Figure S12(d). The spin-degeneracies and splittings on the high symmetry planes $k_x = 0, \pm\pi/a$, $k_y = 0, \pm\pi/b$ and $k_z = 0, \pm\pi/c$, as enforced by the SSG symmetries, are displayed in Figs. S12(e–m).

B. (+−−+)-type spin arrangement at 4c Wyckoff position

The Fe(+−−+)-type spin arrangement at the 4c Wyckoff position yields the AFM phase and hence the Fe sublattice in $CuFePO_5$ is again expected to show spin-degeneracy throughout the Brillouin zone (also see Sec. IIIB 3 of main manuscript). Then the three possible spin arrangements of the Cu sublattice at the 4a Wyckoff position gives rise to SSG symmetries similar to those discussed in Sec. IIIA of main manuscript.

1. *A-type spin arrangement at 4a Wyckoff position*

Figure S13(a) displays A-type spin arrangement of Cu sublattice and (+−−+)-type spin arrangement of Fe sublattice in $CuFePO_5$. From the parent crystallographic space group $\mathbf{G} = \boldsymbol{Pnma}$, the same-spin sublattice transformations for A-type spin arrangement at the 4a Wyckoff position and (+−−+)-type spin arrangement at the 4c Wyckoff position form the *halving* subgroups $\mathbf{H_1} = \tilde{\boldsymbol{C}}^{\boldsymbol{z}}_{\boldsymbol{2h}}$ and $\mathbf{H_5} = \tilde{\boldsymbol{C}}^{\boldsymbol{x}}_{\boldsymbol{2v}}$ respectively (derived and discussed in Secs. IIIA 1 and IIIB 3 of main manuscript). The cosets $\mathbf{G} - \mathbf{H_1}$ and $\mathbf{G} - \mathbf{H_5}$ provide the respective opposite-spin sublattice transformations. Then, the *common* same-spin and opposite-spin sublattice transformations are $\mathbf{H_1} \cap \mathbf{H_5} = \{\, \mathbb{I}, \tilde{m}_{xy} \,\}$ and $(\mathbf{G} - \mathbf{H_1}) \cap (\mathbf{G} - \mathbf{H_5}) = \{\, \tilde{m}_{yz}, \tilde{C}_{2y} \,\}$ respectively. Then the reduced crystallographic space group is given by $\tilde{\boldsymbol{C}}^{\boldsymbol{y}}_{\boldsymbol{2v}} = \{\, \mathbb{I}, \tilde{m}_{xy}, \tilde{m}_{yz}, \tilde{C}_{2y} \,\}$, *isomorphic* to $\boldsymbol{Pn2_1a}$ ($\boldsymbol{C^9_{2v}}$) (also see Table I of main manuscript) [1, 2] and a subgroup of $\mathbf{G}$. The non-trivial spin group becomes:

$$\mathbb{G}_{\mathbf{S}} = \widetilde{\boldsymbol{\mathcal{S}}} \otimes \tilde{\boldsymbol{C}}^{\boldsymbol{y}}_{\boldsymbol{2v}} = [\, \mathfrak{I} \,||\, \{\, \mathbb{I}, \tilde{m}_{xy} \,\}\,] \cup [\, \mathfrak{C}_2 \,||\, \{\, \tilde{m}_{yz}, \tilde{C}_{2y} \,\}\,] \tag{S.7}$$

Thus, A-type spin arrangement on the Cu sublattice and (+−−+)-type spin arrangement on the Fe sublattice in $CuFePO_5$ leads to SSG $\boldsymbol{P\bar{1}n\bar{1}2_1{}^1a}$ (33.146) [4, 15]. From Eqs. (1), (4) and (11) of main manuscript and eq. (S.7), all the resulting spin-degenerate nodal lines and nodal planes across the BZ can be systematically mapped out using the *isomorphic* spin point groups, as discussed in Sec. III of main manuscript. Figure S13(b) shows the BZ along with the IBZ. First-principles calculations reveal fully compensated nature of both Cu and Fe sublattices which is evident from the spin-polarized total DOS as shown in Fig. S13(c). The resulting altermagnetic spin-splitting for these spin arrangements along the IBZ body diagonals is shown in Figure S13(d). The spin-degeneracies and splittings on the high symmetry planes $k_x = 0, \pm\pi/a$, $k_y = 0, \pm\pi/b$ and $k_z = 0, \pm\pi/c$, as enforced by the SSG symmetries, are displayed in Figs. S13(e–m).

2. *C-type spin arrangement at 4a Wyckoff position*

Figure S14(a) displays C-type spin arrangement of Cu sublattice and (+−−+)-type spin arrangement of Fe sublattice in $CuFePO_5$. From the parent crystallographic space group $\mathbf{G} = \boldsymbol{Pnma}$, the same-spin sublattice transformations for A-type spin arrangement at the 4a Wyckoff position and (+−−+)-type spin arrangement at the 4c Wyckoff position form the *halving* subgroups $\mathbf{H_2} = \tilde{\boldsymbol{C}}^{\boldsymbol{y}}_{\boldsymbol{2h}}$ and $\mathbf{H_5} = \tilde{\boldsymbol{C}}^{\boldsymbol{x}}_{\boldsymbol{2v}}$ respectively (derived and discussed in Secs. IIIA 2 and IIIB 3 of main manuscript). The cosets $\mathbf{G} - \mathbf{H_2}$ and $\mathbf{G} - \mathbf{H_5}$ provide the respective opposite-spin sublattice transformations. Then, the *common* same-spin and opposite-spin sublattice transformations are $\mathbf{H_2} \cap \mathbf{H_5} = \{\, \mathbb{I}, \tilde{m}_{zx} \,\}$ and $(\mathbf{G} - \mathbf{H_2}) \cap (\mathbf{G} - \mathbf{H_5}) = \{\, \tilde{m}_{yz}, \tilde{C}_{2z} \,\}$ respectively. Then the reduced crystallographic space group is given by $\tilde{\boldsymbol{C}}^{\boldsymbol{z}}_{\boldsymbol{2v}} = \{\, \mathbb{I}, \tilde{m}_{zx}, \tilde{m}_{yz}, \tilde{C}_{2z} \,\}$, *isomorphic* to $\boldsymbol{Pnm2_1}$ ($\boldsymbol{C^7_{2v}}$) (also see Table I of main manuscript) [1, 2] and a subgroup of $\mathbf{G}$. The non-trivial spin group becomes:

$$\mathbb{G}_{\mathbf{S}} = \widetilde{\boldsymbol{\mathcal{S}}} \otimes \tilde{\boldsymbol{C}}^{\boldsymbol{z}}_{\boldsymbol{2v}} = [\, \mathfrak{I} \,||\, \{\, \mathbb{I}, \tilde{m}_{zx} \,\}\,] \cup [\, \mathfrak{C}_2 \,||\, \{\, \tilde{m}_{yz}, \tilde{C}_{2z} \,\}\,] \tag{S.8}$$

Thus, C-type spin arrangement on the Cu sublattice and (+−−+)-type spin arrangement on the Fe sublattice in $CuFePO_5$ leads to SSG $\boldsymbol{P\bar{1}n^1m\bar{1}2_1}$ (31.126) [4, 15]. From Eqs. (1), (7) and (11) of main manuscript and eq. (S.8), all the resulting spin-degenerate nodal lines and nodal planes across the BZ can be systematically mapped out using the *isomorphic* spin point groups, as discussed in Sec. III of main manuscript. Figure S14(b) shows the BZ along with the IBZ. First-principles calculations reveal fully compensated nature of both Cu and Fe sublattices which is evident from the spin-polarized total DOS as shown in Fig. S14(c). The resulting altermagnetic spin-splitting for these spin arrangements along the IBZ body diagonals is shown in Figure S14(d). The spin-degeneracies and splittings on the high symmetry planes $k_x = 0, \pm\pi/a$, $k_y = 0, \pm\pi/b$ and $k_z = 0, \pm\pi/c$, as enforced by the SSG symmetries, are displayed in Figs. S14(e–m).

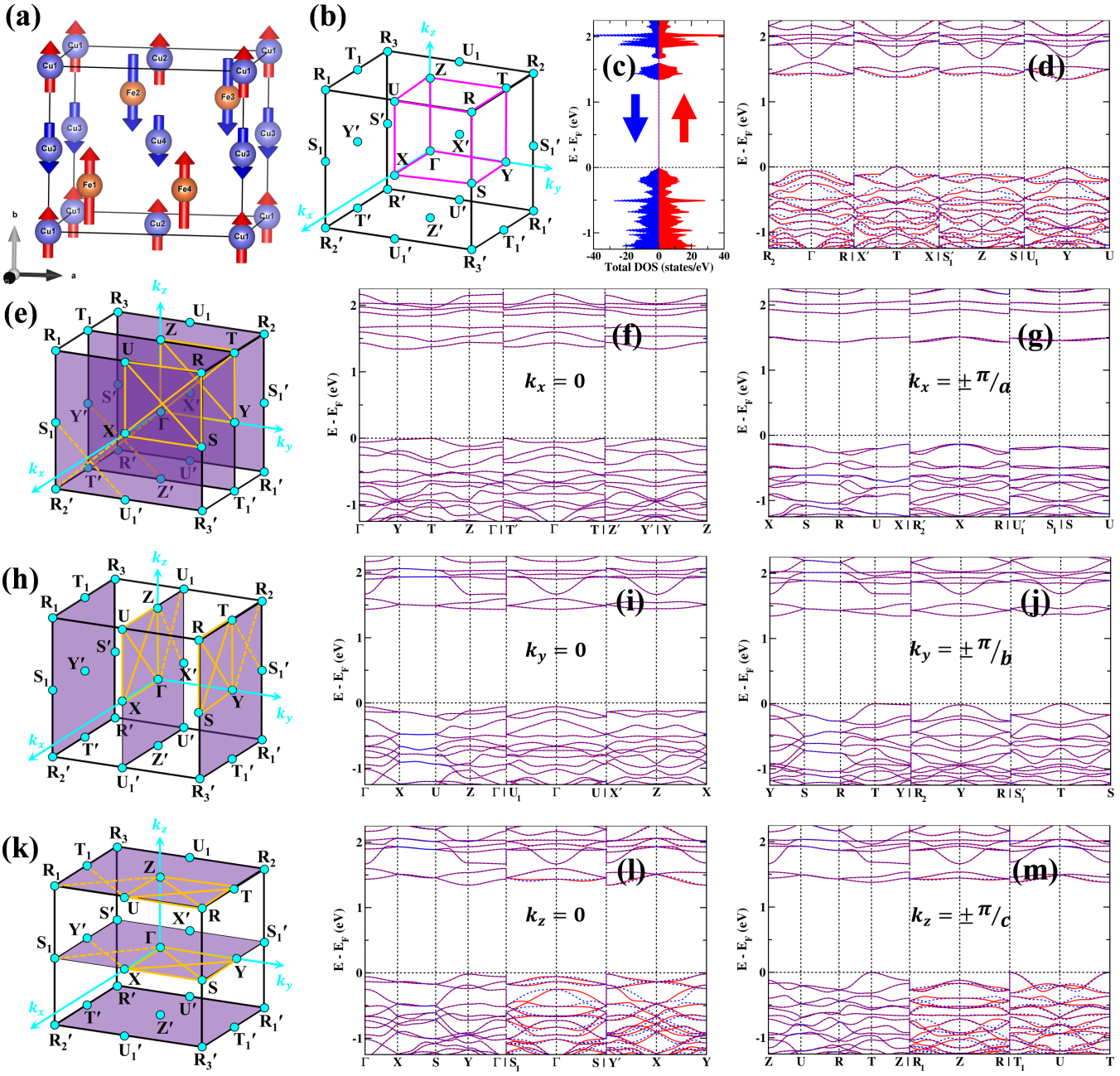

FIG. S13. (a) The Cu and Fe sublattices with A-type and Fe(+−−+)-type spin arrangement respectively. Only the magnetic atoms are shown for visual clarity. (b) *Primitive* orthorhombic Brillouin zone (BZ) with the high-symmetry points shown as cyan dots and the irreducible Brillouin zone (IBZ) marked by magenta lines. (c) Spin-polarized electronic total density of states (TDOS) of $CuFePO_5$. (d) Spin-polarized electronic band structure of $CuFePO_5$ along body diagonals of the IBZ showing spin-splitting, characteristic of the altermagnetic phase. (e) BZ with the $k_x = 0$ and $k_x = \pm\frac{\pi}{a}$ planes highlighted in purple. The high-symmetry directions on the respective planes have been highlighted by orange lines and the spin-polarized electronic band structures of $CuFePO_5$ along these lines have been shown in (f) and (g). (h-j) The same for $k_y = 0$ and $k_y = \pm\frac{\pi}{b}$ planes. (k-m) The same for $k_z = 0$ and $k_z = \pm\frac{\pi}{c}$ planes. In (e), (h) and (k), the solid orange lines denote paths within the IBZ while the broken orange lines denote paths outside the IBZ.

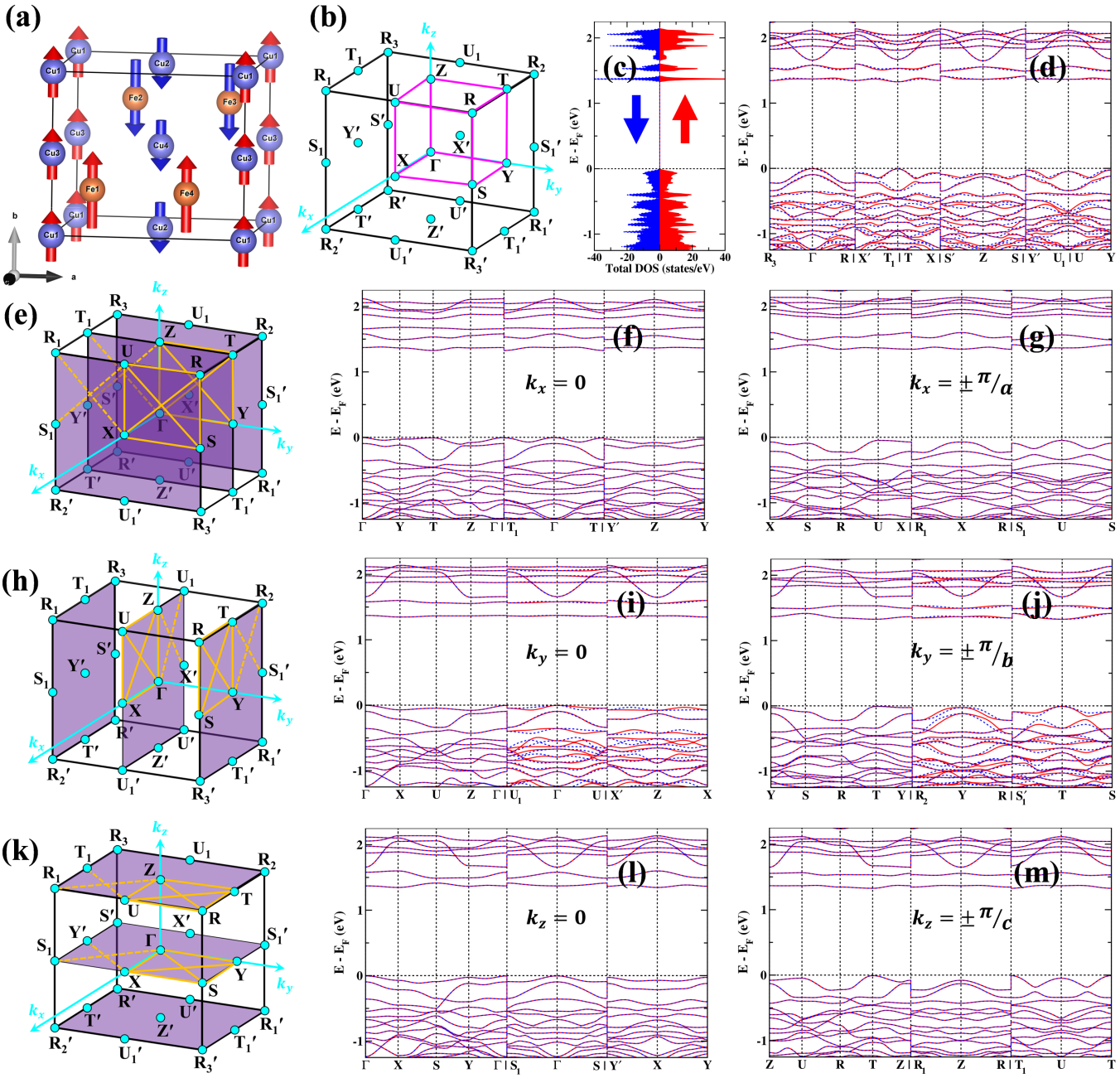

FIG. S14. (a) The Cu and Fe sublattices with C-type and Fe(+−−+)-type spin arrangement respectively. Only the magnetic atoms are shown for visual clarity. (b) *Primitive* orthorhombic Brillouin zone (BZ) with the high-symmetry points shown as cyan dots and the irreducible Brillouin zone (IBZ) marked by magenta lines. (c) Spin-polarized electronic total density of states (TDOS) of $CuFePO_5$. (d) Spin-polarized electronic band structure of $CuFePO_5$ along body diagonals of the IBZ showing spin-splitting, characteristic of the altermagnetic phase. (e) BZ with the $k_x = 0$ and $k_x = \pm\frac{\pi}{a}$ planes highlighted in purple. The high-symmetry directions on the respective planes have been highlighted by orange lines and the spin-polarized electronic band structures of $CuFePO_5$ along these lines have been shown in (f) and (g). (h-j) The same for $k_y = 0$ and $k_y = \pm\frac{\pi}{b}$ planes. (k-m) The same for $k_z = 0$ and $k_z = \pm\frac{\pi}{c}$ planes. In (e), (h) and (k), the solid orange lines denote paths within the IBZ while the broken orange lines denote paths outside the IBZ.

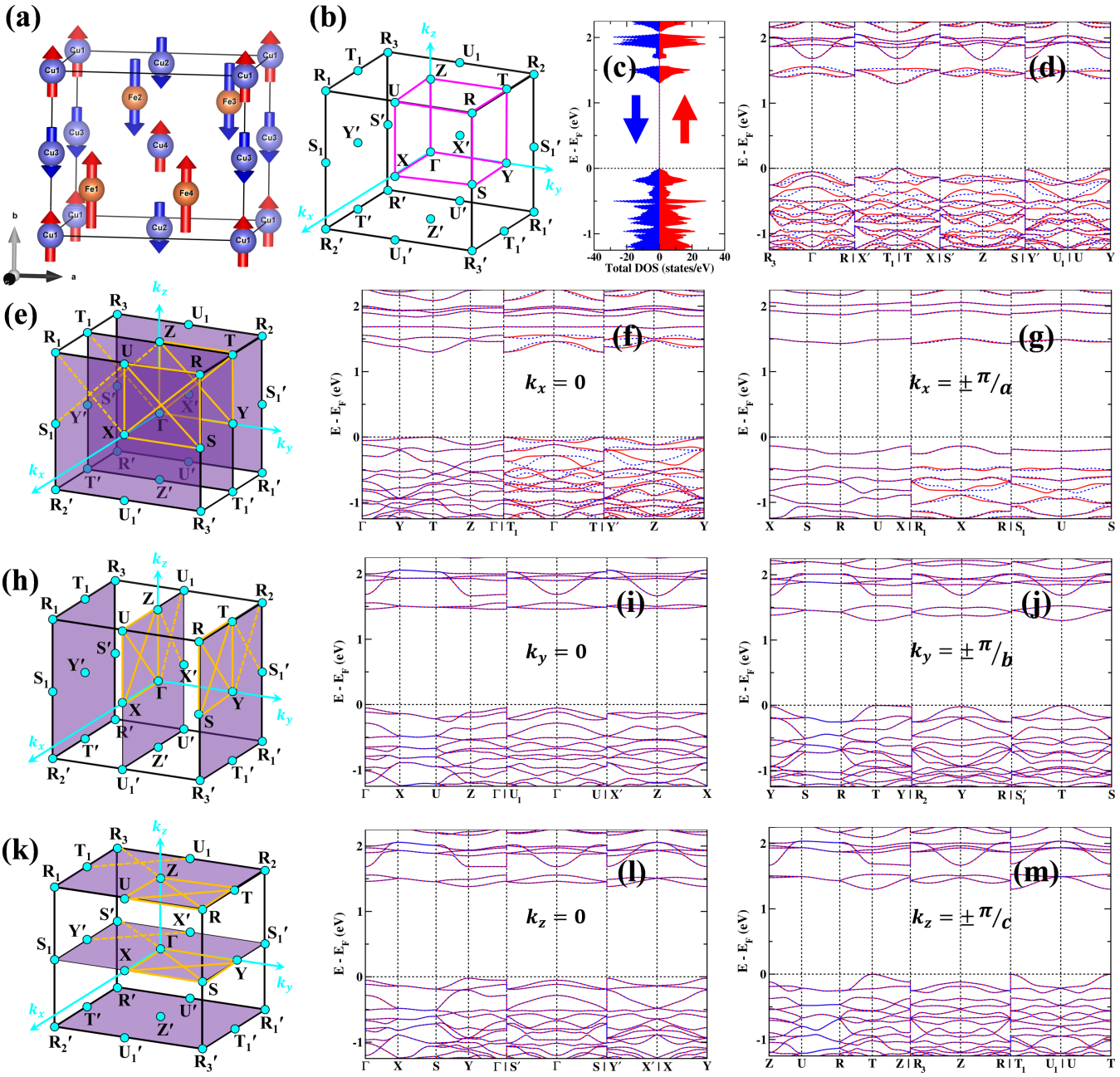

FIG. S15. (a) The Cu and Fe sublattices with G-type and Fe(+−−+)-type spin arrangement respectively. Only the magnetic atoms are shown for visual clarity. (b) *Primitive* orthorhombic Brillouin zone (BZ) with the high-symmetry points shown as cyan dots and the irreducible Brillouin zone (IBZ) marked by magenta lines. (c) Spin-polarized electronic total density of states (TDOS) of $CuFePO_5$. (d) Spin-polarized electronic band structure of $CuFePO_5$ along body diagonals of the IBZ showing spin-splitting, characteristic of the altermagnetic phase. (e) BZ with the $k_x = 0$ and $k_x = \pm\frac{\pi}{a}$ planes highlighted in purple. The high-symmetry directions on the respective planes have been highlighted by orange lines and the spin-polarized electronic band structures of $CuFePO_5$ along these lines have been shown in (f) and (g). (h-j) The same for $k_y = 0$ and $k_y = \pm\frac{\pi}{b}$ planes. (k-m) The same for $k_z = 0$ and $k_z = \pm\frac{\pi}{c}$ planes. In (e), (h) and (k), the solid orange lines denote paths within the IBZ while the broken orange lines denote paths outside the IBZ.

3. G-type spin arrangement at 4a Wyckoff position

Figure S15(a) displays G-type spin arrangement of Cu sublattice and (+−−+)-type spin arrangement of Fe sublattice in $CuFePO_5$. From the parent crystallographic space group $\mathbf{G} = \boldsymbol{Pnma}$, the same-spin sublattice transformations for A-type spin arrangement at the 4a Wyckoff position and (+−−+)-type spin arrangement at the 4c Wyckoff position form the *halving* subgroups $\mathbf{H_3} = \tilde{\boldsymbol{C}}^{\boldsymbol{x}}_{\boldsymbol{2h}}$ and $\mathbf{H_5} = \tilde{\boldsymbol{C}}^{\boldsymbol{x}}_{\boldsymbol{2v}}$ respectively (derived and discussed in Secs. IIIA 3 and IIIB 3 of main manuscript). The cosets $\mathbf{G} - \mathbf{H_3}$ and $\mathbf{G} - \mathbf{H_5}$ provide the respective opposite-spin sublattice transformations. Then, the *common* same-spin and opposite-spin sublattice transformations are $\mathbf{H_3} \cap \mathbf{H_5} = \{\mathbb{I}, \tilde{C}_{2x}\}$ and $(\mathbf{G} - \mathbf{H_3}) \cap (\mathbf{G} - \mathbf{H_5}) = \{\tilde{C}_{2y}, \tilde{C}_{2z}\}$ respectively. Then the reduced crystallographic space group is given by $\tilde{\boldsymbol{D}}_{\boldsymbol{2}} = \{\mathbb{I}, \tilde{C}_{2x}, \tilde{C}_{2y}, \tilde{C}_{2z}\}$, *isomorphic* to $\boldsymbol{P2_12_12_1}$ ($\boldsymbol{D_2^4}$) (also see Table I of main manuscript) [1, 2] and a subgroup of $\mathbf{G}$. The non-trivial spin group becomes:

$$\mathbb{G}_{\mathbf{S}} = \tilde{\boldsymbol{\mathcal{S}}} \otimes \tilde{\boldsymbol{D}}_{\boldsymbol{2}} = [\,\mathfrak{I} \,||\, \{\mathbb{I}, \tilde{C}_{2x}\}\,] \cup [\,\mathfrak{C}_2 \,||\, \{\tilde{C}_{2y}, \tilde{C}_{2z}\}\,] \tag{S.9}$$

Thus, G-type spin arrangement on the Cu sublattice and (+−−+)-type spin arrangement on the Fe sublattice in $CuFePO_5$ leads to SSG $\boldsymbol{P\,^1\!2_1\,^{\bar{1}}\!2_1\,^{\bar{1}}\!2_1}$ (19.27) [4, 15]. From Eqs. (1), (10) and (11) of main manuscript and eq. (S.9), all the resulting spin-degenerate nodal lines and nodal planes across the BZ can be systematically mapped out using the *isomorphic* spin point groups, as discussed in Sec. III of main manuscript. Figure S15(b) shows the BZ along with the IBZ. First-principles calculations reveal fully compensated nature of both Cu and Fe sublattices which is evident from the spin-polarized total DOS as shown in Fig. S15(c). The resulting altermagnetic spin-splitting for these spin arrangements along the IBZ body diagonals is shown in Figure S15(d). The spin-degeneracies and splittings on the high symmetry planes $k_x = 0, \pm\pi/a$, $k_y = 0, \pm\pi/b$ and $k_z = 0, \pm\pi/c$, as enforced by the SSG symmetries, are displayed in Figs. S15(e–m).

[1] M. I. Aroyo, J. M. Perez-Mato, C. Capillas, E. Kroumova, S. Ivantchev, G. Madariaga, A. Kirov, and H. Wondratschek, Bilbao Crystallographic Server: I. Databases and crystallographic computing programs, Z. Kristallogr. Cryst. Mater. **221**, 15 (2006).

[2] H. Arnold, M. I. Aroyo, E. F. Bertaut, H. Burzlaff, G. Chapuis, W. Fischer, H. D. Flack, A. M. Glazer, H. Grimmer, B. Gruber, T. Hahn, H. Klapper, E. Koch, P. Konstantinov, V. Kopskỳ, D. B. Litvin, A. Looijenga-Vos, U. Müller, K. Momma, U. Shmueli, B. Souvignier, J. C. H. Spence, P. M. de Wolff, , H. Wondratschek, and H. Zimmermann, *International tables for crystallography volume A: Space-group symmetry*, 2nd ed., edited by M. I. Aroyo (Wiley Online Library, 2016).

[3] D. Litvin and W. Opechowski, Spin groups, Physica **76**, 538 (1974).

[4] D. B. Litvin, Spin point groups, Acta Cryst. A **33**, 279 (1977).

[5] P. Liu, J. Li, J. Han, X. Wan, and Q. Liu, Spin-Group Symmetry in Magnetic Materials with Negligible Spin-Orbit Coupling, Phys. Rev. X **12**, 021016 (2022).

[6] L. Šmejkal, J. Sinova, and T. Jungwirth, Beyond Conventional Ferromagnetism and Antiferromagnetism: A Phase with Nonrelativistic Spin and Crystal Rotation Symmetry, Phys. Rev. X **12**, 031042 (2022).

[7] L. Šmejkal, J. Sinova, and T. Jungwirth, Emerging Research Landscape of Altermagnetism, Phys. Rev. X **12**, 040501 (2022).

[8] Z. Xiao, J. Zhao, Y. Li, R. Shindou, and Z.-D. Song, Spin Space Groups: Full Classification and Applications, Phys. Rev. X **14**, 031037 (2024).

[9] X. Chen, J. Ren, Y. Zhu, Y. Yu, A. Zhang, P. Liu, J. Li, Y. Liu, C. Li, and Q. Liu, Enumeration and Representation Theory of Spin Space Groups, Phys. Rev. X **14**, 031038 (2024).

[10] Y. Jiang, Z. Song, T. Zhu, Z. Fang, H. Weng, Z.-X. Liu, J. Yang, and C. Fang, Enumeration of Spin-Space Groups: Toward a Complete Description of Symmetries of Magnetic Orders, Phys. Rev. X **14**, 031039 (2024).

[11] A. Kitz, Über die Symmetriegruppen von Spinverteilungen Von, Phys. Status Solidi B **10**, 455 (1965).

[12] M. Touaiher and A. El Hajbi, Preparation and characterisation of the compounds $MFePO_5$ (M = Ni, Cu), Adv. Mater. Res. **1**, 215 (1994).

[13] N. El Khayati, R. C. El Moursli, J. Rodríguez-Carvajal, G. André, N. Blanchard, F. Bourée, G. Collin, and T. Roisnel, Magnetic structure of $MFePO_5$ compounds (M = Cu, Ni), Phosphorus Res. Bull. **11**, 107 (2000).

[14] N. El Khayati, R. Cherkaoui El Moursli, J. Rodríguez-Carvajal, G. André, N. Blanchard, F. Bourée, G. Collin, and T. Roisnel, Crystal and magnetic structures of the oxyphosphates $MFePO_5$ (M = Fe, Co, Ni, Cu). Analysis of the magnetic ground state in terms of superexchange interactions, Eur. Phys. J. B **22**, 429 (2001).

[15] X. Chen, Y. Liu, P. Liu, Y. Yu, J. Ren, J. Li, A. Zhang, and Q. Liu, Unconventional magnons in collinear magnets dictated by spin space groups, Nature **640**, 349 (2025).